50272-101

REPORT DOCUMENTATION PAGE	1. REPORT NO. NCEER-91-0008	2.	3. PB92-113828

4. Title and Subtitle
Nonlinear Analysis of Steel Frames with Semi-Rigid Connections Using the Capacity Spectrum Method

5. Report Date
July 2, 1991

6.

7. Author(s)
G.G. Deierlein, S-H. Hsieh, Y-J. Shen and J.F. Abel

8. Performing Organization Rept. No.

9. Performing Organization Name and Address
Department of Structural Engineering
School of Civil and Environmental Engineering
Cornell University
Ithaca, New York 14853

10. Project/Task/Work Unit No.

11. Contract(C) or Grant(G) No.
(C) 88-1005A, 89-1201A and 90-1201A
(G) ECE 86-07591

12. Sponsoring Organization Name and Address
National Center for Earthquake Engineering Research
State University of New York at Buffalo
Red Jack Quadrangle
Buffalo, New York 14261

13. Type of Report & Period Covered
Technical Report

14.

15. Supplementary Notes
This research was conducted at Cornell University and was partially supported by the National Science Foundation under Grant No. ECE 86-07591.

16. Abstract (Limit: 200 words)
This report summarizes the development and application of a computeraided system for the inelastic analysis, evaluation, and design of three-dimensional steel frames with semi-rigid connections under static loading. Main components of the work include: 1) development of a model to represent the nonlinear moment-rotation response of partially restrained connections; 2) development of a matrix-based method for incorporating the connection model in a nonlinear finite element program for framed structures; 3) implementation of the connection model in CU-STAND, a workstation based program for interactive analysis and design of steel framed structures; 4) computer implementation of the capacity spectrum method for estimating inelastic seismic response using modal analysis; 5) demonstration of the system for sensitivity studies on the inelastic reponse of a planar frame with semi-rigid connections. Through a case study, overall frame response is found to be relatively insensitive to variations in the connection response parameters. The case study also includes application of the capacity spectrum method to investigate the inelastic limit state under seismic loading and comparisons are made with results based on equivalent static code-based loading.

17. Document Analysis a. Descriptors

b. Identifiers/Open-Ended Terms

EARTHQUAKE ENGINEERING.	INELASTIC ANALYSIS.	INELASTIC RESPONSE.
SEMI-RIGID FRAMES.	CAPACITY SPECTRUM METHOD.	STEEL FRAMES.
NONLINEAR RESPONSE.	THREE DIMENSIONAL FRAMES.	CU-STAND.
COMPUTER PROGRAMS.	STATIC LOADING.	

c. COSATI Field/Group

18. Availability Statement	19. Security Class (This Report)	21. No. of Pages
Release Unlimited	Unclassified	96
	20. Security Class (This Page)	22. Price
	Unclassified	

PB92-113828

NATIONAL CENTER FOR EARTHQUAKE ENGINEERING RESEARCH

State University of New York at Buffalo

Nonlinear Analysis of Steel Frames with Semi-Rigid Connections Using the Capacity Spectrum Method

by

G. G. Deierlein, S-H. Hsieh, Y-J. Shen and J. F. Abel

Department of Structural Engineering
School of Civil and Environmental Engineering
Cornell University
Ithaca, New York 14853

Technical Report NCEER-91-0008

July 2, 1991

This research was conducted at Cornell University and was partially supported by the National Science Foundation under Grant No. ECE 86-07591.

Nonlinear Analysis of Steel Frames with Semi-Rigid Connections Using the Capacity Spectrum Method

by

G.G. Deierlein[1], S-H. Hsieh[2], Y-J. Shen[2] and J.F. Abel[3]

July 2, 1991

Technical Report NCEER-91-0008

NCEER Project Numbers 88-1005A, 89-1201A and 90-1201A

NSF Master Contract Number ECE 86-07591

1 Assistant Professor, School of Civil and Environmental Engineering, Cornell University
2 Graduate Research Assistant, School of Civil and Environmental Engineering, Cornell University
3 Professor, School of Civil and Environmental Engineering, Cornell University

NATIONAL CENTER FOR EARTHQUAKE ENGINEERING RESEARCH
State University of New York at Buffalo
Red Jacket Quadrangle, Buffalo, NY 14261

PREFACE

The National Center for Earthquake Engineering Research (NCEER) is devoted to the expansion and dissemination of knowledge about earthquakes, the improvement of earthquake-resistant design, and the implementation of seismic hazard mitigation procedures to minimize loss of lives and property. The emphasis is on structures and lifelines that are found in zones of moderate to high seismicity throughout the United States.

NCEER's research is being carried out in an integrated and coordinated manner following a structured program. The current research program comprises four main areas:

- Existing and New Structures
- Secondary and Protective Systems
- Lifeline Systems
- Disaster Research and Planning

This technical report pertains to Program 1, Existing and New Structures, and more specifically to system response investigations.

The long term goal of research in Existing and New Structures is to develop seismic hazard mitigation procedures through rational probabilistic risk assessment for damage or collapse of structures, mainly existing buildings, in regions of moderate to high seismicity. The work relies on improved definitions of seismicity and site response, experimental and analytical evaluations of systems response, and more accurate assessment of risk factors. This technology will be incorporated in expert systems tools and improved code formats for existing and new structures. Methods of retrofit will also be developed. When this work is completed, it should be possible to characterize and quantify societal impact of seismic risk in various geographical regions and large municipalities. Toward this goal, the program has been divided into five components, as shown in the figure below:

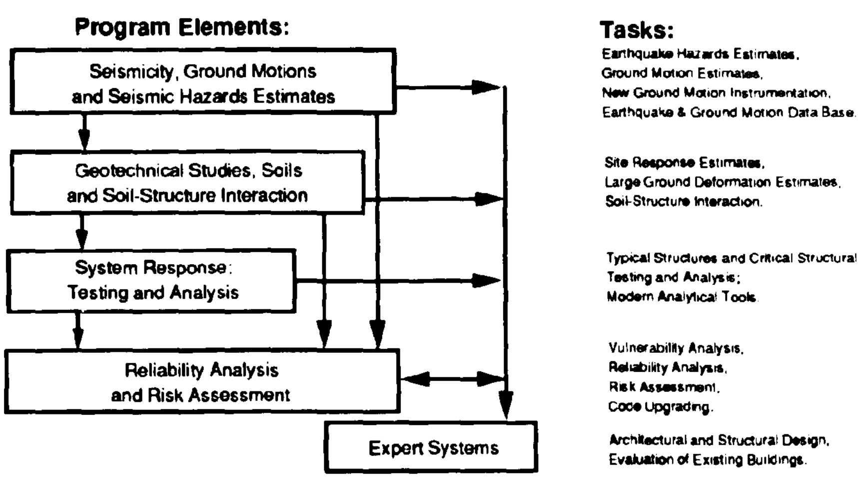

System response investigations constitute one of the important areas of research in Existing and New Structures. Current research activities include the following:

1. Testing and analysis of lightly reinforced concrete structures, and other structural components common in the eastern United States such as semi-rigid connections and flexible diaphragms.
2. Development of modern, dynamic analysis tools.
3. Investigation of innovative computing techniques that include the use of interactive computer graphics, advanced engineering workstations and supercomputing.

The ultimate goal of projects in this area is to provide an estimate of the seismic hazard of existing buildings which were not designed for earthquakes and to provide information on typical weak structural systems, such as lightly reinforced concrete elements and steel frames with semi-rigid connections. An additional goal of these projects is the development of modern analytical tools for the nonlinear dynamic analysis of complex structures.

This report addresses one of the key questions in the analysis of structures for earthquake loads: how to estimate nonlinear response for design purposes without performing numerous nonlinear time-history analyses for a series of ground motions. The capacity spectrum method was employed to predict the nonlinear load and deformation levels of steel frames for given response spectra using static analyses. Typical steel frames were analyzed using a recently developed semirigid zero-length connection model. Both material and geometric nonlinearities are incorporated in the program. The results demonstrate the importance of the effects of nonlinear geometric effects on the inelastic limit state behavior. The model and the capacity spectrum method form a useful tool for estimating the nonlinear response of partially restrained steel structures.

Abstract

This report summarizes the development and application of a computer-aided system for the inelastic analysis, evaluation, and design of three-dimensional steel frames with semi-rigid connections under static loading. Main components of the work include: (1) development of a model to represent the nonlinear moment-rotation response of partially restrained connections, (2) development of a matrix-based method for incorporating the connection model in a nonlinear finite element program for framed structures, (3) implementation of the connection model in CU-STAND, a workstation based program for interactive analysis and design of steel framed structures, (4) computer implementation of the capacity spectrum method for estimating inelastic seismic response using modal analysis, and (5) demonstration of the system for sensitivity studies on the inelastic response of a planar frame with semi-rigid connections.

The connection model is based on a four parameter power equation. Based on calibration to existing experimental data, sets of normalized parameters are proposed for use where more exact values based on test data are not available. Through a case study, overall frame response is found to be relatively insensitive to variations in the connection response parameters. The case study also includes application of the capacity spectrum method to investigate the inelastic limit state under seismic loading and comparisons are made with results based on equivalent static code-based loading.

TABLE OF CONTENTS

LIST OF ILLUSTRATIONS

LIST OF TABLES

SECTION 1
INTRODUCTION

The influence of semi-rigid connection behavior on the overall response of structures has long been recognized, but it has been common practice to treat connections in steel structures as either perfectly rigid or pinned. One reason for this is the lack of accurate and convenient methods to include semi-rigid connection effects directly in analysis and design. The need for including the effects of connection flexibility in the analysis of building systems is particularly important for use in limit state design methods and in evaluating the seismic risk for new and existing structures.

This report summarizes the development and application of a computer-aided analysis and design system to evaluate the nonlinear response of steel structures with partially restrained connections to static loads. Included is an application of the capacity spectrum method for evaluating the inelastic response of structures to earthquake forces. The inelastic response is calculated using a 2nd-order inelastic analysis program which includes the effect of nonlinear connection flexibility.

1.1 Nonlinear Analysis System for Frames with Semi-Rigid Connections

The nonlinear analysis formulation for 3D frames with semi-rigid connections is implemented in a computer-aided system called CU-STAND (Static Analysis and Design). CU-STAND is one of three interactive-graphics workstation based programs developed at Cornell University for the nonlinear analysis and design of two- and three-dimensional steel framed structures. The other two programs are CU-PREPF (a Preprocessor for Framed Structures) and CU-QUAND (Earthquake Analysis and Design). Further information regarding the three programs is included in References 1-4.

The analysis methods in CU-STAND are based on a finite element discretization of the structure into beam-column line elements. The analysis includes provisions for modeling nonlinear response due to large displacements (geometric effects), member plastification (inelastic effects), and connection flexibility. The analysis also includes options for modeling rigid floor diaphragms and can handle both proportional and nonproportional loading. Finally, as described below, the program includes features for generating the capacity spectrum response curve for an equivalent static earthquake loading.

1.2 Capacity Spectrum Method

Currently, structural design for earthquake forces is usually based on an elastic analysis where some approximation is used to account for the inelastic response of the structure. The loading used in the elastic analyses may be based on equivalent static forces obtained from design codes such as the Uniform Building Code, or they may be obtained from a modal analysis using a design spectrum. The advantage of these methods is that they are relatively straightforward and convenient for design. The disadvantage, however, is that most elastic design methods offer little information regarding the inelastic response of the structure. Hence, the rationale for such methods lies largely in the reliability obtained through a track record of reasonable performance for standard building configurations with adequate ductility. As such, elastic design methods are not well suited for structures of irregular configuration or for evaluating the damage susceptibility of existing buildings to various levels of seismic forces.

Sophisticated transient dynamic inelastic analysis methods are available which represent the best available technology for simulating the response of structures subjected to strong earthquake loadings. However, a drawback of such methods is the time and expense required to perform the analysis and interpret the results for design. Therefore, while advanced dynamic analyses are useful for investigations under a specific set of circumstances, they are currently still considered too cumbersome for most routine applications.

Freeman [5] has developed a method, called the capacity spectrum method, which uses a static inelastic analysis to estimate the seismic performance of a structure. The advantage of this method over other equivalent static analyses is that it provides more information on the degree of inelastic deformation (damage) which is expected to occur. Recently, Chrysostomou et al. [6] implemented a modified version of this method to study the effects of degrading infill walls on the nonlinear seismic response of steel frames.

The **capacity spectrum** is a structural property which provides a relationship between the period (or frequency) and acceleration levels of the structure corresponding to various stages of loading. The **demand spectrum** (response or design spectrum) represents the demand of the ground motion in terms of the induced elastic response of a single degree-of-freedom oscillator to a particular earthquake. As shown in Fig. 1.1 through superposition of the capacity spectrum and the demand spectrum, the maximum response and the inelastic period of vibration can be approximated. The response predicted using the capacity spectrum can be related to other information obtained in the analysis to estimate the deformations and level of damage in the structure.

1.3 Scope and Organization of Report

The scope of this report is to describe the theoretical basis and analytical formulations of the analysis techniques used to evaluate the inelastic response of steel structures with partially restrained connections and to present a case study which demonstrates application of the method. This work is part of an ongoing NCEER project to develop and use workstation based computer-aided analysis methods for the design and evaluation of new and existing structures. Included in the description of the analysis system is: a) development of the nonlinear connection model and calibration to test data, b) formulation of the nonlinear beam-column element stiffness with semi-rigid connections, and c) theoretical development and computer implementation of the capacity spectrum method.

A case study of a low rise steel frame is presented which includes: a) a systematic investigation of the sensitivity of overall structural response to variations in the assumed semi-rigid connection properties, and b) application of the capacity spectrum method to evaluate the inelastic response of frames with partially restrained connections using design spectrum curves.

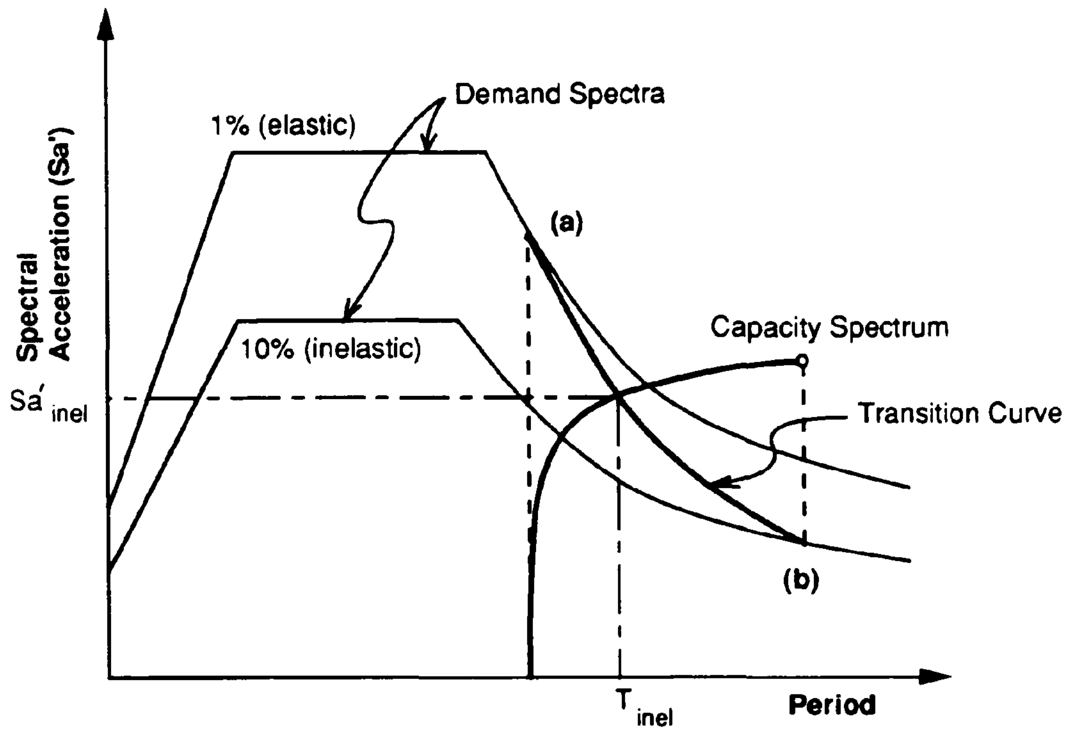

FIGURE 1-1 Capacity and Demand Spectra.

SECTION 2
NONLINEAR CONNECTION MODEL

Many investigations into the behavior and modeling of semi-rigid connections have been reported [7]. Although most of them have only considered in-plane behavior of connections, they still form the essential basis of accounting for connection flexibility in the analysis and design of structures. In this work, the connection behavior is modeled by a nonlinear equation for moment-rotation response which is calibrated to test data and normalized for use in design.

2.1 Moment-Rotation Model

Many techniques have been proposed for representing the moment-rotation behavior of semi-rigid connections, some based on simple linear approximations and others on more sophisticated nonlinear functions. The model used in this work is based on a nonlinear equation first presented by Richard and Abbott [8], and later by Kishi et al. [9]. Using this model, the moment-rotation relationship of the connection is given by the following equation:

$$M = \frac{(K_e - K_p)\theta}{\left(1 + \left|\frac{(K_e - K_p)\theta}{M_o}\right|^n\right)^{1/n}} + K_p\theta \tag{2.1}$$

In Eq. 2.1, M is the moment corresponding to the connection rotation, θ. The parameters, K_e, K_p, and M_o, are independent variables which are related to the moment-rotation behavior as shown in Fig. 2-1, and n controls the shape of the curve. This model was chosen because it represents observed experimental data well, it is convenient to implement in the computer program described below, and the four parameters are derived from a rational interpretation of the connection response. Another advantage of this model is that it encompasses more simple models. For example, Eq. 2.1 becomes a simple linear model if $K_e = K_p$, an elastic-plastic model if $K_p = 0$, and a bilinear model if n is large.

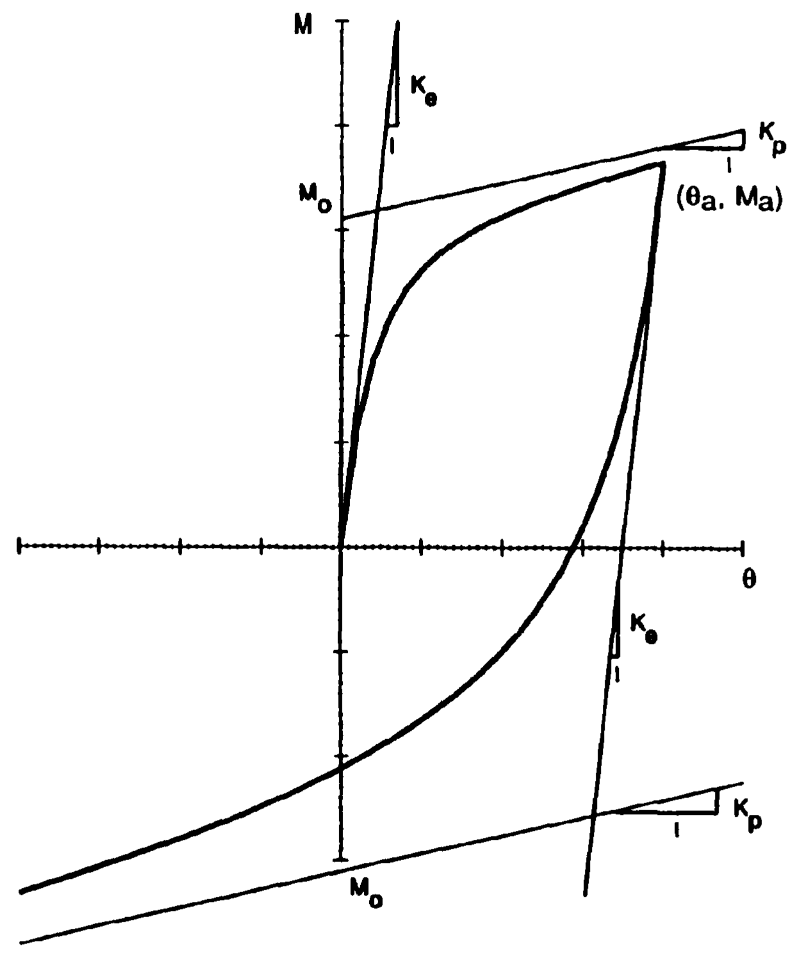

FIGURE 2-1 Moment-rotation Model for Inelastic Connection Response

To allow for unloading of the connections associated with nonproportional loading and inelastic force redistribution, the unloading curve shown in Fig. 2-1 was developed by Hsieh [10]. This portion of the moment-rotation curve is given by the following equation, where the peak moments and rotations reached during the initial loading are M_a and θ_a:

$$M = M_a - \frac{(K_e-K_p)(\theta_a-\theta)}{\left(1+\left|\frac{(K_e-K_p)(\theta_a-\theta)}{2M_o}\right|^n\right)^{1/n}} - K_p(\theta_a-\theta) \tag{2.2}$$

For use in an incremental finite element analysis, the tangent stiffness of the connection is obtained by differentiating Eq. 2.1 with respect to θ, resulting in the following expression:

$$K_t = \frac{dM}{d\theta} = \frac{(K_e-K_p)}{\left(1+\left|(K_e-K_p)\frac{\theta}{M_o}\right|^n\right)^{(n+1)/n}} + K_p \tag{2.3}$$

2.2 Determination of Parameters. The four parameters of the model may be determined by several means according to the specific needs in analysis and design. If experimental data are available, the most precise representation is obtained through curve-fitting the model directly to the data. Where test data are not available, as is typically the case in practice, the parameters may be determined using analytic formulations for the connection strength and stiffness if the connection details are known. In design practice, however, it is usually the case that the connection details may not be known until after the structural members have been sized. As described below, a third method proposed for determining the parameters is based on using standardized curves to provide the general shape of the response curve and analytic (design) methods to calculate the nominal connection strength. The standardized curves are obtained from statistical analysis of normalized curves which were curve-fit to experimental data previously collected by Kishi & Chen [11] and Goverdhan [12]. A summary of the connection types and abbreviations for the connections considered is given in Table 2-1

TABLE 2-1 Connection Nomenclature

Abbreviation	Connection Type
SWA	Single Web-Angle Connections (All bolted)
DWA	Double Web-Angle Connections (All bolted)
TSAW	Top- and Seat-Angle Connections with Double Web-Angles (All bolted)
TSA	Top- and Seat-Angle Connections (All bolted)
EEP	Extended End-Plate Connections (All bolted without column stiffeners)
EEPS	Extended End-Plate Connections (All bolted with column stiffeners)
FEP	Flush End-Plate Connections (All bolted without column stiffeners)
FEPS	Flush End-Plate Connections (All bolted with column stiffeners)
HP	Header Plate Connections (All bolted)

Curve-fitting from experimental data. An optimization approach utilizing the conjugate-gradient method is used to find a set of parameters (M_o, K_e, K_p, and n) which gives the best curve-fit to experimental response data. In this method, the conjugate directions are used to search for the minimum of the objective function in a N-dimensional problem space. Using a method analogous to the Gram-Schmidt orthogonalization procedure, each conjugate direction used for a new search is set up by a linear combination of all the previous search directions and the newly determined gradient of the objective function. This method converges quadratically.

The optimization searches are performed in a four-dimensional space to obtain the parameters, M_o, K_e, K_p, and n, from Eq. 2.1. This is an unconstrained optimization problem and the objective (error) function is expressed by the following:

$$W = \sum_{i=1}^{X} \left((m_i - M_i) / \sqrt{1+K_{ti}^2}\right)^2 \qquad (2.4)$$

in which

X = number of experimental test data,

m_i = moment value of i-th test data,

M_i = moment value calculated from Eq. 2.1 at the rotation value of the i-th test data, and

K_{ti} = the tangent stiffness calculated from Eq. 2.3 at the rotation of the i-th test data.

As shown in Fig. 2-2, the error term in Eq. 2.4 is simply the orthogonal distance between a test data point and the moment-rotation curve. It has been found that the curve-fitting results are sensitive to the initial value of the parameter n assumed in the calculation. Therefore, ten different initial values of n from 0.1 to 5.0 are tried for each set of test data and the resulting values of W are compared to obtain the "best" curve-fit. In addition, the maximum moment reported in the test, the initial stiffness, and the final stiffness calculated directly from test data are used for initial values of M_0, K_e, and K_p, respectively. An example of the curve-fitting results for top- and seat-angle connections with double web angles (TSAW) is shown in Fig. 2-3. Comparisons between the experimental data and curve-fitting results for other connections are included in Appendix A. In general, the curve-fitting results produce good agreement with the experimental data.

Standardized connection reference curves. In structural design practice, it is unlikely that specific information regarding the connection details will be known during preliminary design, and even during final design, this information may not be available until after the structural members have been sized. Since connection flexibility will affect the structural response and therefore the required member sizes, there is a need to develop some means of accounting for connection behavior in the analysis during the design process before final member sizes are selected. One solution is to use standardized connection reference curves which are based on test data and normalized for use in design.

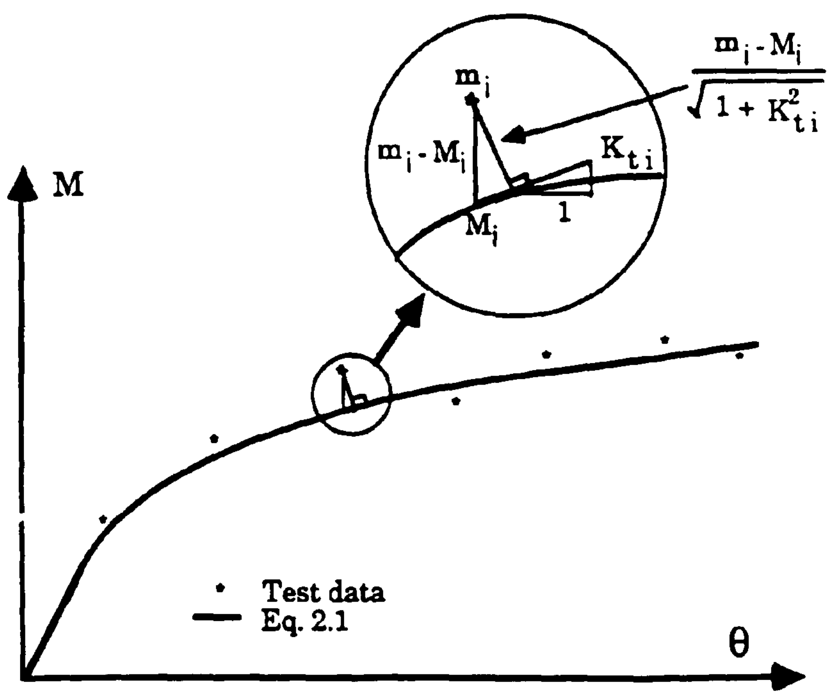

FIGURE 2-2 Calculation of Distance Between Test Data and Eq. 2.1

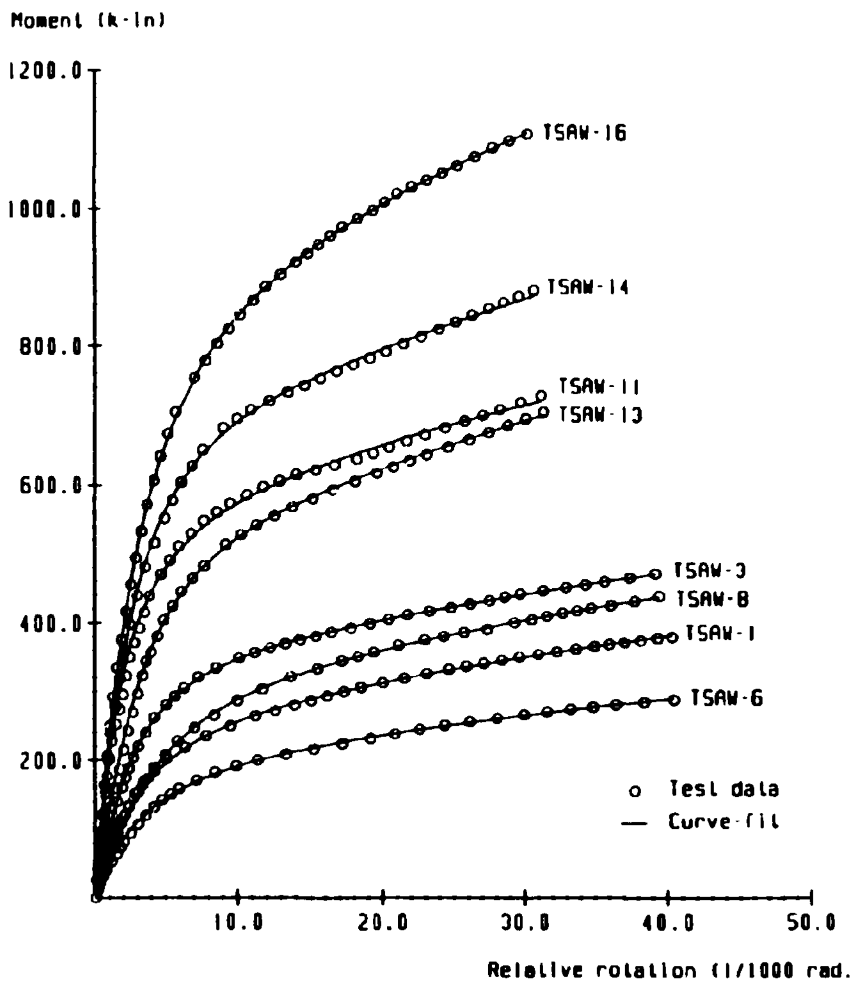

FIGURE 2-3 Comparison Between Curve-fitting Results and Experimental Results for TSAW Connections

To generalize Eqs. 2.1, 2.2, and 2.3 for design, the moment-rotation expressions are first normalized with respect to a reference value of moment which is defined herein as the nominal connection capacity, M_{cn}. The normalized expressions are identical to Eqs. 2.1, 2.2, and 2.3 except that M, M_o, M_a, K_e, and K_p are replaced by $M'=M/M_{cn}$, $M_o'=M_o/M_{cn}$, $M_a'=M_a/M_{cn}$, $K_e'=K_e/M_{cn}$ and $K_p'=K_p/M_{cn}$, respectively. The resulting normalized expression for Eq. 2.1 is the following:

$$M' = \frac{\left(K_e' - K_p'\right)\theta}{\left(1 + \left|\frac{K_e' - K_p'\theta}{M_o'}\right|^n\right)^{1/n}} + K_p'\theta \qquad (2.5)$$

An example is presented below to illustrate how the normalized parameters (K_e', K_p', M_o', and n) are determined for top- and seat-angle connections with double web angles (TSAW connections).

Using the curve-fitting results presented previously in Fig. 2-3, each of the curves were normalized by a value of M_{cn} equal to the moment resisted at an applied rotation of 0.02 radian. This value was chosen after considering several alternate normalization schemes, further details of which are reported by Hsieh [10]. The normalization procedure results in the set of curves shown in Fig. 2-4a. For a given type of connection, this procedure provides a convenient means of condensing the data from a large number of tests by eliminating variations due to scale (strength) effects.

From the normalized curves shown in Fig. 2-4a, the three standard reference curves shown in Fig. 2-4b were developed for each connection type. The AVE curve is obtained by curve-fitting the normalized model (Eq. 2.4) to a set of points equal to the average values of M' determined from sets of curves such as shown in Fig. 2-4a. The averages were evaluated for values of rotation between 0.002 and 0.05 radian. In this case, the error function used in the curve fitting was equal to the sum of the squares of the value of moment between the average value points and the calculated values:

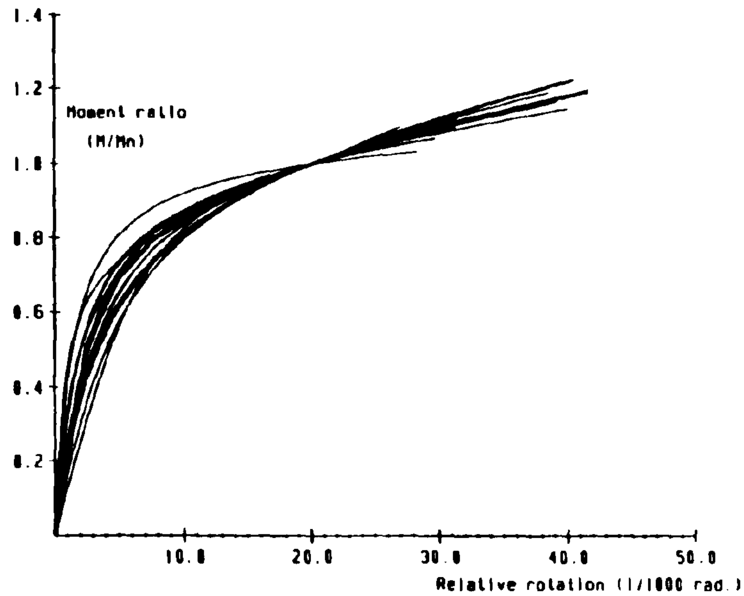

a) Normalized Curves

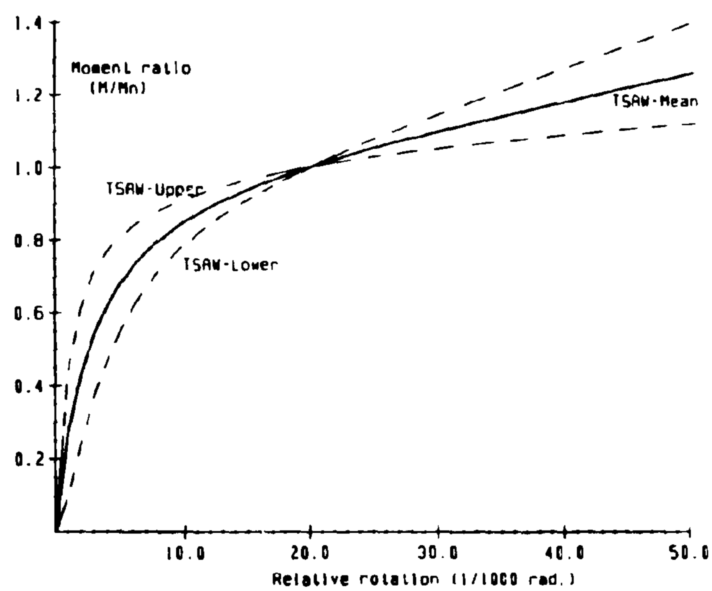

b) Standardized Curves

FIGURE 2-4 Normalized and Standardized Moment-rotation Connection Curves for TSAW connections

$$W = \sum_{i=1}^{X} \left(\frac{m_i}{M_{cn}} - \frac{M_i}{M_{cn}} \right)^2 \qquad (2.6)$$

$\frac{m_i}{M_{cn}}$: normalized moment for each average value

$\frac{M_i}{M_{cn}}$: calculated normalized moment

As described by Shen [13], a weighting function was applied to the objective function which improved the accuracy of the curve-fitting over the region where connection rotations are less than .02 radians.

The upper and lower curves in Fig. 2-4b reflect a variation from the average curve of plus or minus two standard deviations. The UPPER curve is generated by fitting Eq. 2-4 to the set of points equal to m_i (average) plus two standard deviations for rotations less than 0.02 radian and m_i (average) minus two standard deviations for rotations greater than 0.02 radian. The LOWER curve is fit to the average value minus two standard deviations for connection rotations less than 0.02 radian and the average plus two standard deviations for rotations greater than 0.02 radian. Assuming the variation in connection response is random and normally distributed (which as shown by Shen [13] is a reasonable assumption), the region between the upper and lower curves in Fig. 2-4b encompasses roughly 95% of the sampled data. Standardized curves were developed for other connection types, and parameters for the AVE, UPPER, and LOWER curves for all the connection types considered are shown in Table 2-2. Plots of the AVE curve for each connection type are shown in Fig. 2-5.

2.3 Design Reference Curve

For design purposes, one reference curve which represents the average response for all connection types was developed. This curve was developed using the same procedure as described above for calculating the average curves, except that in this case, the family of curves which was used to generate the final curve consisted of the AVE curves for each connection

Table 2-2. Parameters for Normalized Connection Curves

Type of Connection Curve	M_0'	K_c'	K_p'	n
SWA-UPPER	1.05	167.83	3.33	1.47
SWA-AVE	1.08	113.34	9.13	1.26
SWA-LOWER	0.74	65.46	19.52	2.43
DWA-UPPER(A441)	0.85	464.40	8.62	1.37
DWA-AVE(A441)	0.71	231.03	17.96	1.16
DWA-LOWER(A441)	1.79	42.20	10.34	2.45
DWA-UPPER(A36)	0.98	439.20	1.57	2.28
DWA-AVE(A36)	0.93	253.29	6.32	1.41
DWA-LOWER(A36)	0.90	85.75	10.04	2.23
TSAW-UPPER	0.93	435.91	4.06	1.62
TSAW-AVE	0.90	266.47	7.53	1.40
TSAW-LOWER	0.80	132.31	12.02	2.00
TSA-UPPER	1.02	399.10	1.88	1.27
TSA-AVE	0.96	226.16	8.23	1.16
TSA-LOWER	0.69	91.60	17.48	2.40
EEP-UPPER	0.88	502.63	6.60	1.98
EEP-AVE	0.94	229.73	8.45	1.19
EEP-LOWER	0.74	73.71	14.16	3.72
EEPS-UPPER	1.00	338.68	0.01	1.80
EEPS-AVE	1.05	184.68	1.59	1.54
EEPS-LOWER	0.93	88.36	6.28	2.99
FEP-UPPER	1.02	275.91	1.46	1.56
FEP-AVE	0.99	200.76	4.63	1.43
FEP-LOWER	0.90	119.21	8.12	1.93
FEPS-UPPER	1.00	367.50	2.43	1.44
FEPS-AVE	0.98	238.25	5.35	1.33
FEPS-LOWER	0.89	121.44	8.86	2.03
HP-UPPER	0.92	226.75	0.00	2.77
HP-AVE	0.81	143.83	13.82	1.45
HP-LOWER	2.74	74.13	22.33	0.67

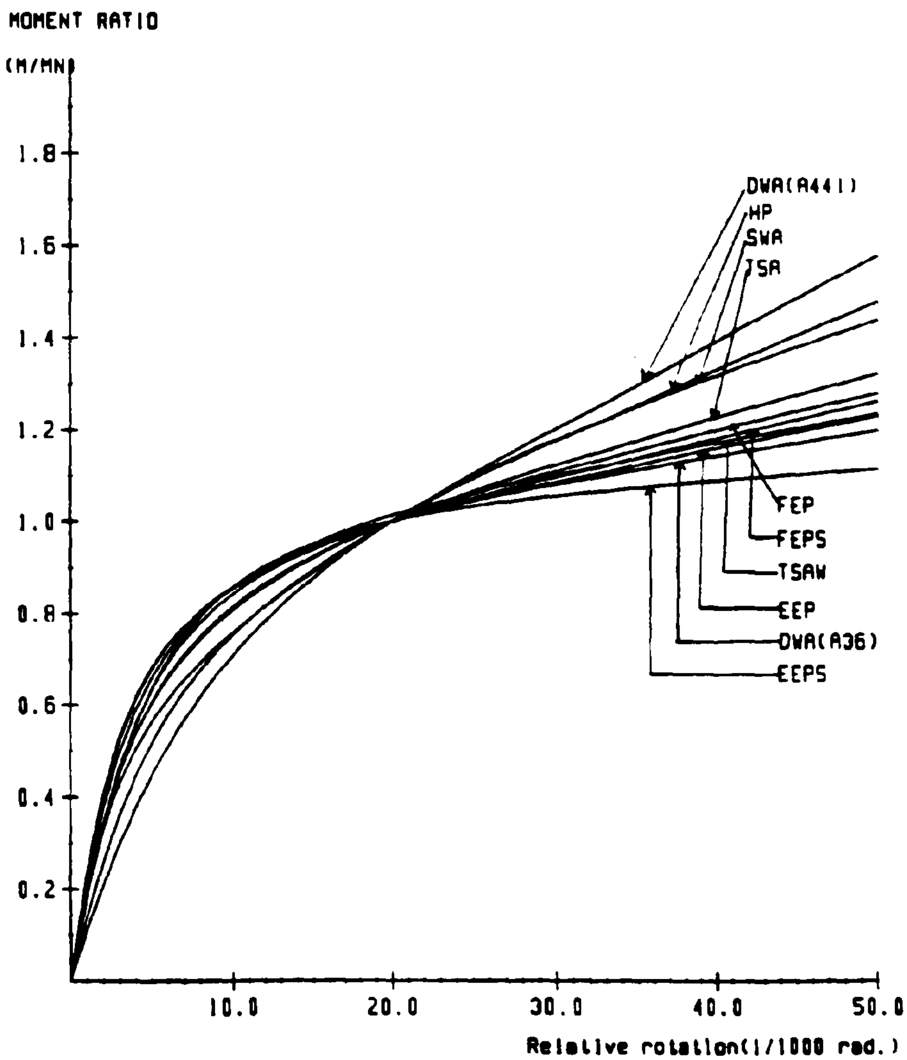

FIGURE 2-5 The AVE. Curves for all Types of Connections

type (Fig. 2-5). The model parameters obtained based on all nine types of connections are $K_e' = 191$, $K_p' = 8.5$, $M_o' = 0.91$ and $n = 1.4$. Because the single web angle (SWA), double web angle (DWA), and header plate (HP) connections are usually not used where a significant moment resistant is desired, the parameters for the design curve were recalculated excluding these connections. The parameters based on the remaining five types of connections are: $K_e' = 222$, $K_p' = K_e'/50 = 4.0$, $M_o' = 0.98$ and $n = 1.35$. For design, these values are rounded off to the following: $K_e' = 200$, $K_p' = 4$, $M_o' = 1.0$ and $n = 1.4$.

The resulting design reference curve is compared to the average curves for the five types of connections in Fig. 2-6. When $\theta < 0.02$ radian, there is not much variation between the various connection curves and the design curve is very close to the average. However, for $\theta > 0.02$, there are greater differences between the different connection types and the design curve (specifically K_p') was purposely chosen to be near the lower bound of response.

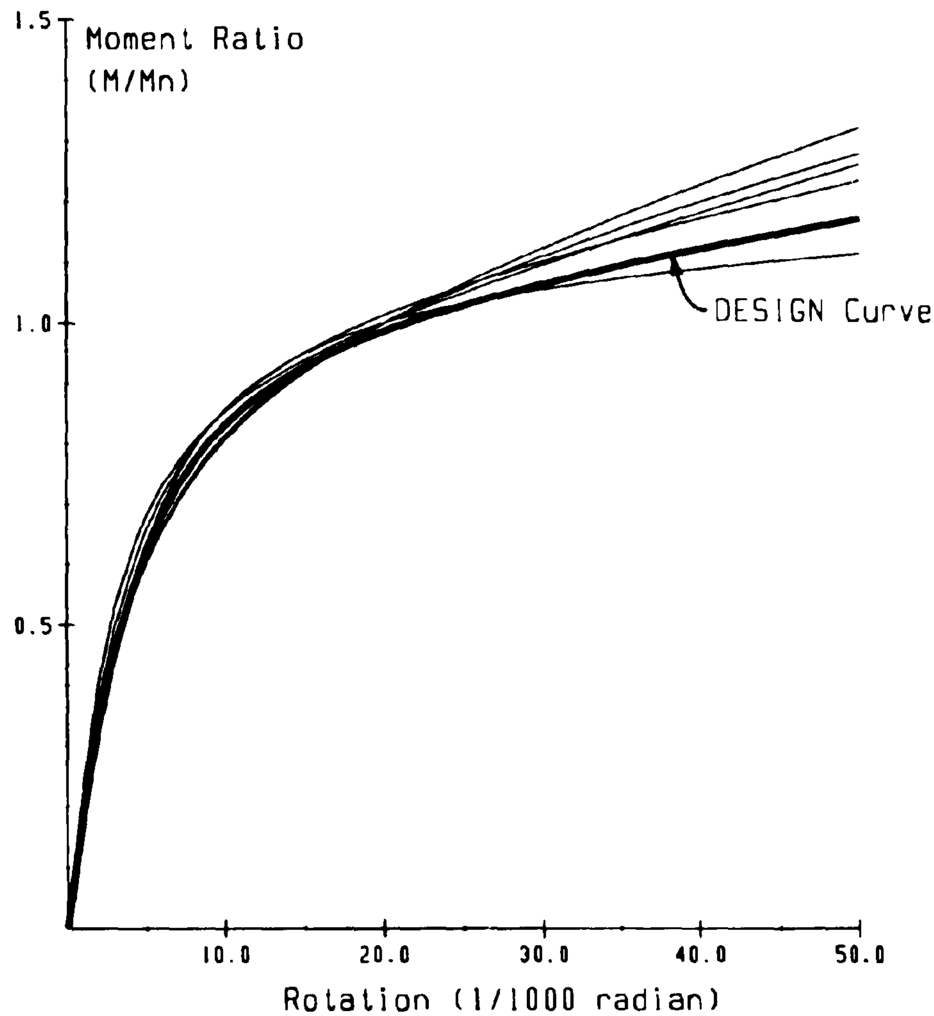

FIGURE 2-6 Standard Design Reference Curve

SECTION 3
FINITE ELEMENT ANALYSIS OF SEMI-RIGID FRAMES

As noted previously, the connection model was incorporated into the program, CU-STAND for the nonlinear analysis of three-dimensional steel frames with semi-rigid connections subjected to static loading. An important aspect of the model implementation is that it did not require fundamental changes to the existing geometric and material nonlinear model for the elastic-plastic beam-column elements in CU-STAND. The following is a summary of the finite element formulation and computer implementation in CU-STAND.

3.1 Modeling of the Beam-Column Element

The beam-column element in CU-STAND includes both geometric and material nonlinearities. A brief review of the formulation is given in this section; more details are contained in Reference [2].

Beam-columns are modeled as line elements with twelve degrees-of-freedom, consisting of three translations and three rotations, at each end of the element. Common beam theory assumptions, such as homogeneous and isotropic material, plane sections remain plane, doubly symmetric prismatic sections with no cross section distortion, and small strain theory, are employed in the formulation of the element stiffness. In linear elastic analyses, the element stiffness is the conventional linear elastic stiffness matrix, $[k_e]$ (see, for example, Chapter 4 in [14]). For second order analyses, geometric nonlinearities are handled through the use of element geometric stiffness matrices $[k_g]$ and an updated Lagrangian formulation. The nodal coordinates and the terms in $[k_g]$ are updated at the end of each incremental/iterative load step. For inelastic analyses, material nonlinearities are included through the use of element plastic reduction matrices $[k_p]$ which are based on a three parameter yield surface for modeling cross-section plastification due to axial load and major- and minor-axis bending. This is a concentrated plasticity model approach where it is assumed that zero-length plastic hinges form at the end of each element. Details of the stiffness matrices $[k_e]$, $[k_g]$, and $[k_p]$ are provided in Reference [2].

Using this approach, the incremental element equilibrium equations can be written in the following form:

$$\{ds\} = [\,[k_e] + [k_g] + [k_p]\,]\,\{du\} = [k_t]\,\{du\} \qquad (3.1)$$

In Eq. 3.1, $\{ds\}$ is the vector of incremental element end forces; $\{du\}$ is the vector of incremental element displacements; $[k_e]$, $[k_g]$, and $[k_p]$ are elastic, geometric, and plastic reduction matrices, respectively; and $[k_t]$ is the resulting element tangent stiffness matrix. Depending on the type of analysis (e.g., 1st-order or 2nd-order, elastic or inelastic), $[k_g]$ and/or $[k_p]$ may not be included in the analysis.

The global incremental equilibrium equations are written as the following:

$$\{dP\} = [K_t]\,\{dU\} \qquad (3.2)$$

In Eq. 3.2, $\{dP\}$ is the incremental load vector applied on the entire structure, $\{dU\}$ is the global incremental displacement vector, and $[K_t]$ is the global stiffness matrix obtained by assembling the transformed element tangent stiffness matrices, $[k_t]$. As described in Reference [2], CU-STAND has several solution method options for Eq. 3.2 and force recovery procedures which include provisions to limit cumulative errors during inelastic loading.

3.2 Modeling of Semi-rigid Connections

Zero-length connection elements are used to permit relative flexural rotations between connected members; the connections do not allow for relative torsional rotation or translational displacements. When a semi-rigid connection is specified at one end of a member, the global rotational degrees-of-freedom at the corresponding structural node are associated with the connection element. The corresponding local rotational degrees-of-freedom between the member end and connection are treated as additional global unknowns of the structural system and are included in the global equilibrium equations (i.e. , Eq. 3.2). Condensation is not used here because it is not as efficient for nonlinear analyses in which stiffness matrices are updated many times. In the formulation, the additional rotational degrees-of-freedom described above are always measured with respect to the local member coordinates even though they are treated as global unknowns in Eq. 3.2.

To introduce the local degrees-of-freedom into the global solution system, the conventional element transformation matrices are modified for the elements with semi-rigid connections. The modified matrices are used to transform the element stiffness matrices from the local to the global coordinate system with some of the unknowns retaining their local coordinate reference axes.

A key advantage of this approach is that the existing nonlinear formulation for the beam-column elements is unaffected. This avoids the difficulty (particularly for three-dimensional problems) of directly formulating the connection flexibility into the nonlinear element stiffness matrices, $[k_g]$ and $[k_p]$. The use of separate connection elements also facilitates further modifications to the connection model (for example, to account for the finite size of the connection or for including additional connection degrees-of-freedom). On the other hand, a disadvantage of this approach is that it increases the total number of degrees-of-freedom in the global system of equations. However, this disadvantage is becoming less significant with the continuing improvement of computer hardware.

Example Formulation. An example is presented to demonstrate the formulation and transformation of the beam-column element stiffnesses with nonlinear connection flexibility. A portion of a three-dimensional structure discretized in a global coordinate system with orthogonal axes X, Y, and Z is shown in Fig. 3-1. The connection elements **Aa** and **Bb** connect the beam **ab** to the nodes **A** and **B**. For clarity, the connection elements are shown "exploded" to a finite length but are actually zero-length. The local (or element) coordinate system of the beam **ab** with orthogonal axes x, y, and z is also shown. In general, the local coordinate axes (x, y, z) are arbitrarily oriented with respect to the global coordinate axes (X, Y, Z).

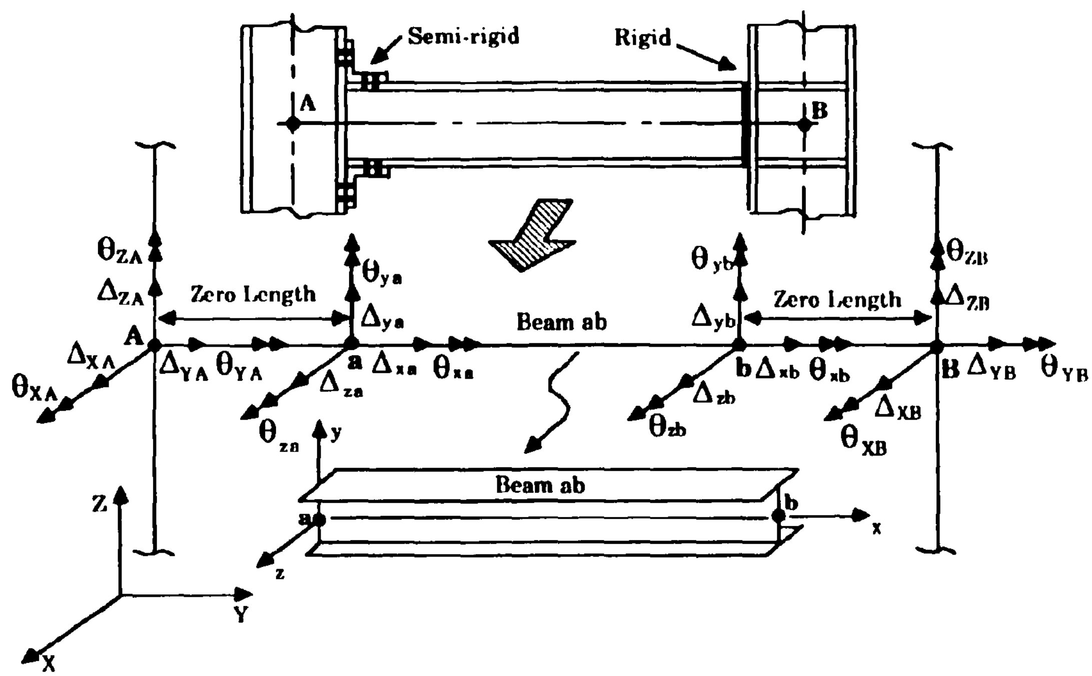

FIGURE 3-1 Structural Discretization for a Beam-Column With Zero Length Connections

In Fig. 3-1, the degrees-of-freedom (DOF's) at nodes **A** and **B** are represented using the displacement components in the global coordinates, and the DOF's of beam **ab** are shown in terms of local coordinates at both ends of the beam. In the displacement components, Δ_{ij} and θ_{ij}, the first subscript **i** refers to the global or local component axes and the second subscript **j** refers to the global or member node designation. These subscripts are also used in developing the expressions for the forces and moments, F_{ij} and M_{ij}, respectively.

In the example considered, it is assumed that the connection element **Aa** includes both major-axis and minor-axis rotational flexibility while the connection **Bb** is rigid. Aside from major- and minor-axis flexure, no other deformations are allowed in the connection **Aa**.

Matrix Notations: The following matrix notations are used in the formulation:

$[\gamma]_{3x3}$ = the conventional rotation matrix of beam **ab**

$[I]_{2x2}$ = identity matrix

$$[G]_{6x6} = \begin{bmatrix} [\gamma]_{3x3} & 0 \\ 0 & [\gamma]_{3x3} \end{bmatrix}$$

$[T1]_{4x6}$ = the first four rows of $[G]$

$[T2]_{2x6}$ = the last two rows of $[G]$

Member Transformation Matrix. At end **a** of beam **ab**, relative major- and minor-axis rotations between the beam end and the node to which it is connected (θ_{ya} and θ_{za}) are allowed. Transfer of the global DOF's at node **A** into the local coordinate system is done by the following equation:

$$\begin{Bmatrix} \Delta_{xa} \\ \Delta_{ya} \\ \Delta_{za} \\ \theta_{xa} \end{Bmatrix} = \begin{bmatrix} & & \\ & T_1 & \\ & & \end{bmatrix}_{4x6} \begin{Bmatrix} \Delta_{XA} \\ \Delta_{YA} \\ \Delta_{ZA} \\ \theta_{XA} \\ \theta_{YA} \\ \theta_{ZA} \end{Bmatrix} \tag{3.3}$$

Adding θ_{ya} and θ_{za} to Eq. 6, results in the following equation which relates the local beam DOF's to the mixed (local and global) DOF's considered in the global system of equations:

$$\begin{Bmatrix} \Delta_{xa} \\ \Delta_{ya} \\ \Delta_{za} \\ \theta_{xa} \\ \theta_{ya} \\ \theta_{za} \end{Bmatrix} = \begin{bmatrix} \begin{bmatrix} & & \\ & T_1 & \\ & & \end{bmatrix}_{4x6} & 0 \\ 0 & [\,I\,]_{2x2} \end{bmatrix} \begin{Bmatrix} \Delta_{XA} \\ \Delta_{YA} \\ \Delta_{ZA} \\ \theta_{XA} \\ \theta_{YA} \\ \theta_{ZA} \\ \theta_{ya} \\ \theta_{za} \end{Bmatrix}$$

$$= [G1]_{6x8}\,\{D1\}_{8x1} \tag{3.4}$$

Similarly, equilibrium gives the following transformation of forces from the local to the mixed global system:

$$
\begin{Bmatrix} F_{xa} \\ F_{ya} \\ F_{za} \\ M_{xa} \\ M_{ya} \\ M_{za} \end{Bmatrix} = \begin{bmatrix} \begin{bmatrix} & & \\ & T_1 & \\ & & \end{bmatrix}_{4x6} & 0 \\ 0 & [\,I\,]_{2x2} \end{bmatrix} \begin{Bmatrix} F_{XA} \\ F_{YA} \\ F_{ZA} \\ M_{XA} \\ M_{YA} \\ M_{ZA} \\ M_{ya} \\ M_{za} \end{Bmatrix}
$$

$$
= [G1]_{6x8}\,\{F1\}_{8x1} \qquad (3.5)
$$

Since, in this particular case, no connection flexibility is considered at end **b** of the beam, the displacement and force transformations are given in the following standard forms:

$$
\begin{Bmatrix} \Delta_{xb} \\ \Delta_{yb} \\ \Delta_{zb} \\ \theta_{xb} \\ \theta_{yb} \\ \theta_{zb} \end{Bmatrix} = \begin{bmatrix} & & \\ & G & \\ & & \end{bmatrix} \begin{Bmatrix} \Delta_{XB} \\ \Delta_{YB} \\ \Delta_{ZB} \\ \theta_{XB} \\ \theta_{YB} \\ \theta_{ZB} \end{Bmatrix}
$$

$$
= [G2]_{6x6}\,\{D2\}_{6x1} \qquad (3.6)
$$

$$\begin{Bmatrix} F_{xb} \\ F_{yb} \\ F_{zb} \\ M_{xb} \\ M_{yb} \\ M_{zb} \end{Bmatrix} = \begin{bmatrix} \\ \\ & G & \\ \\ \\ \end{bmatrix} \begin{Bmatrix} F_{XB} \\ F_{YB} \\ F_{ZB} \\ M_{XB} \\ M_{YB} \\ M_{ZB} \end{Bmatrix}$$

$$= [G2]_{6x6} \{F2\}_{6x1} \tag{3.7}$$

Using Eqs. 3.4 to 3.7, the transformation matrix of beam **ab** can be written as the following:

$$[\Gamma b]_{12x14} = \begin{bmatrix} [G1]_{6x8} & 0 \\ & \\ 0 & [G2]_{6x6} \end{bmatrix} \tag{3.8}$$

This matrix is then used to transform the element stiffness matrix from the local to the global system, where the equilibrium equations for beam **ab** in the global system are given as follows:

$$\begin{Bmatrix} F1 \\ \text{-----} \\ F2 \end{Bmatrix}_{14x1} = \begin{bmatrix} \\ Kb \\ \\ \end{bmatrix}_{14x14} \begin{Bmatrix} D1 \\ \text{-----} \\ D2 \end{Bmatrix}_{14x1} \tag{3.9}$$

In Eq. 3.9, $[Kb] = [\Gamma b]^T [k_t] \; [\Gamma b]$, $[k_t]$ = element tangent stiffness matrix of the beam **ab** (Eq. 3.1), and {F1}, {F2}, {D1}, and {D2} are defined in Eqs. 3.4 - 3.7. Note that θ_{ya} and θ_{za} in {D1} are local rotations at end **a** of the beam and M_{ya} and M_{za} in {F1} are the corresponding member end moments measured in local coordinates.

<u>Stiffness Matrix of Connection **Aa**:</u> Given K_Z = the tangent stiffness of connection **Aa** for major-axis (z-axis) bending, Ky = the tangent stiffness for minor-axis (y-axis) bending, and the relative connection rotations are $(\theta_{zA} - \theta_{za})$ and $(\theta_{yA} - \theta_{ya})$, respectively, the equilibrium equations for connection element **Aa** are given as the following:

$$\begin{Bmatrix} M_{yA} \\ M_{zA} \\ M_{ya} \\ M_{za} \end{Bmatrix} = \begin{bmatrix} K_y & 0 & -K_y & 0 \\ 0 & K_z & 0 & -K_z \\ -K_y & 0 & K_y & 0 \\ 0 & -K_z & 0 & K_z \end{bmatrix} \begin{Bmatrix} \theta_{yA} \\ \theta_{zA} \\ \theta_{ya} \\ \theta_{za} \end{Bmatrix} = [kc]_{4x4} \begin{Bmatrix} \theta_{yA} \\ \theta_{zA} \\ \theta_{ya} \\ \theta_{za} \end{Bmatrix} \tag{3.10}$$

In Eq. 3.10, [kc] is the tangent stiffness of connection **Aa** measured in local coordinates.

<u>Transformation of Connection Stiffness:</u> From compatibility at node **A**, the internal (local) displacements are related to the global displacements by the following equation in which $[T_2]$ was defined previously:

$$\begin{Bmatrix} \theta_{yA} \\ \theta_{zA} \end{Bmatrix} = \begin{bmatrix} & & \\ & T_2 & \\ & & \end{bmatrix}_{2x6} \begin{Bmatrix} \Delta_{XA} \\ \Delta_{YA} \\ \Delta_{ZA} \\ \theta_{XA} \\ \theta_{YA} \\ \theta_{ZA} \end{Bmatrix} \tag{3.11}$$

Note that the first three columns of $[T_2]$ are null for the present case of infinitesimal joint size and non-eccentric member ends.

Adding θ_{ya} and θ_{za} to Eq. 3.11, and using a similar transformation for forces, the displacement and force transformations at the connection are given by Eqs. 3.12 and 3.13:

$$\begin{Bmatrix} \theta_{yA} \\ \theta_{zA} \\ \theta_{ya} \\ \theta_{za} \end{Bmatrix} = \begin{bmatrix} \begin{bmatrix} & T_2 & \end{bmatrix}_{2x6} & 0 \\ 0 & [\,I\,]_{2x2} \end{bmatrix} \begin{Bmatrix} \Delta_{XA} \\ \Delta_{YA} \\ \Delta_{ZA} \\ \theta_{XA} \\ \theta_{YA} \\ \theta_{ZA} \\ \theta_{ya} \\ \theta_{za} \end{Bmatrix}$$

$$= [\Gamma c]_{4x8}\,\{D1\}_{8x1} \qquad (3.12)$$

$$\begin{Bmatrix} M_{yA} \\ M_{zA} \\ M_{ya} \\ M_{za} \end{Bmatrix} = \begin{bmatrix} \begin{bmatrix} & T_2 & \end{bmatrix}_{2x6} & 0 \\ 0 & [\,I\,]_{2x2} \end{bmatrix} \begin{Bmatrix} F_{XA} \\ F_{YA} \\ F_{ZA} \\ M_{XA} \\ M_{YA} \\ M_{ZA} \\ M_{ya} \\ M_{za} \end{Bmatrix}$$

$$= [\Gamma c]_{4x8}\,\{F1\}_{8x1} \qquad (3.13)$$

Using the transformation matrix $[\Gamma c]$ from Eqs. 3.12 and 3.13, the equilibrium equations for connection **Aa** in the global system are given as the following, where $[Kc]_{8x8} = [\Gamma c]^T_{8x4}\,[kc]_{4x4}\,[\Gamma c]_{4x8}$ and $[kc]$ = element stiffness matrix of connection **Aa** per Eq. 3.10:

$$
\begin{Bmatrix} F_{XA} \\ F_{YA} \\ F_{ZA} \\ M_{XA} \\ M_{YA} \\ M_{ZA} \\ M_{ya} \\ M_{za} \end{Bmatrix} = \begin{bmatrix} & & \\ & K_c & \\ & & \end{bmatrix}_{8x8} \begin{Bmatrix} \Delta_{XA} \\ \Delta_{YA} \\ \Delta_{ZA} \\ \theta_{XA} \\ \theta_{YA} \\ \theta_{ZA} \\ \theta_{ya} \\ \theta_{za} \end{Bmatrix} \qquad (3.14)
$$

Extensions for Other Situations: The transformation procedure demonstrated above in Eqs. 3.3-3.14 can be modified to cover connections with only major- or minor-axis rotational flexibility and for beam-column elements with connections at both ends. All of these cases are included in the computer implementation in CU-STAND.

3.3 Computer Implementation

In addition to implementing the connection model described above, control menu's were added in CU-STAND for definition of the connection parameters and to assign connections by graphically attaching them to specific members. One of the connection editor menus is shown in Fig. 3-2 through which the user can interactively assign the four parameters which define the shape of the connection model and the nominal connection strength, M_{cn}. Based on the user input, a plot of the moment rotation curve for the connection is shown in the viewports in the upper left portion of the screen. In the program, the four connection parameters can be either specified directly by the user, chosen from a library of values for standard connection types, or generated from moment-rotation data using the built-in curve-fitting routine described previously. The nominal connection strength, M_{cn}, can be specified either as an absolute value or as some fraction of the plastic moment of the member, M_{pb}, to which the connection is attached . The latter option is particularly suited to an iterative design process where connection and member properties are unknown at the outset and updated in the course of design.

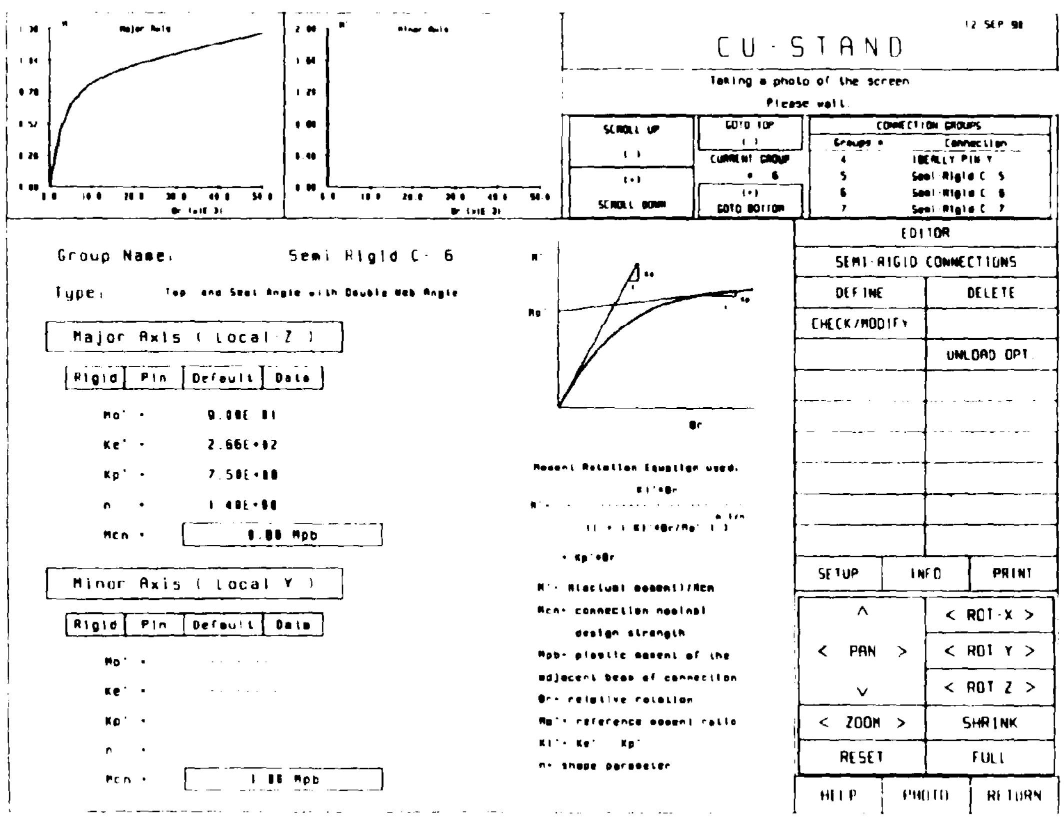

FIGURE 3-2 Menu Page for Defining Connection Properties

SECTION 4
CAPACITY SPECTRUM METHOD

The capacity spectrum method provides a means for incorporating inelastic structural response into a seismic response spectrum procedure which is amenable to engineering practice. This method was first presented by Freeman [5] for the design and evaluation of reinforced structures and was recently applied to steel framed structures with concrete infill walls by Chrysostomou et. al., [6]. The essence of this method entails calculation of the capacity spectrum which relates the natural period of vibration of the structure to the level of induced response. As will be described below, the capacity spectrum is used together with elastic demand (response) spectra to obtain an approximation of the actual response.

The capacity spectrum is calculated using an incremental inelastic static analysis in which the structure is loaded with equivalent static earthquake forces. The load vector may be obtained from procedures based on a code such as the Uniform Building Code or from a modal analysis. The magnitude of the vector is not important, but the distribution of forces should reflect the inertial earthquake loading corresponding to the dominant mode(s) of vibration. In the analysis, the equivalent static load is applied incrementally, and at each step, the fundamental period of vibration is calculated to reflect the decreasing stiffness associated with the inelastic deformation of the structure. Also, the total applied load at each step is used to calculate an equivalent spectral acceleration.

The spectral acceleration (Sa) is related to the vector of maximum structural accelerations ($\ddot{x}$) in the direction of earthquake motion by the following equation:

$$\{\ddot{x}\} = \Gamma \, Sa \, \{\phi\} \tag{4.1}$$

In this equation, $\{\phi\}$ is the eigenvector corresponding to the fundamental mode of vibration, and Γ is the modal participation factor for this mode, given as the following:

$$\Gamma = \frac{[\phi]\,[M]\,\{d\}}{[\phi][M]\{\phi\}} = \frac{\Sigma\, m_i \phi_i}{\Sigma\, m_i\, \phi_i^2} \tag{4.2}$$

In Eq. 4.2, [M] is the matrix of lumped masses, m_i, and {d} is a unit vector. Note that the matrix multiplication is reduced to a summation by taking advantage of the diagonal mass matrix. The vector of inertial loads {P} is calculated by multiplying the nodal accelerations $\{\ddot{x}\}$ by the masses as given by the following equation:

$$\{P\} = [M]\{\ddot{x}\} = \frac{\Sigma\, m_i\, \phi_i}{\Sigma m_i\, \phi_i^2}\, Sa\, [M]\, \{\phi\} \tag{4.3}$$

The total base shear, V, which is equal to the summation of the inertial loads can then be related to the spectral acceleration by the following equation:

$$V = \Sigma\, P_i = [(\Sigma m_i\, \phi_i)^2 \,/\, (\Sigma\, m_i\, \phi_i^2)]\; Sa \tag{4.4}$$

Rearranging Eq. 4.4, and expressing the spectral acceleration as a fraction of gravity, (i.e., Sa' = Sa/g) the following expression is obtained:

$$Sa' = [(\Sigma\, m_i\, \phi_i^2) \,/\, (\Sigma\, m_i\, \phi_i)^2]\; V \,/\, g \tag{4.5}$$

For the implementation used in this research, the fundamental period and mode shape were calculated directly using the mass and stiffness matrices and a standard eigensolution routine. Alternatively, assuming that the displaced shape of the structure under the equivalent static load vector approximates the first mode shape, Eq. 4.5 can be approximated by the following equation in which Δ_i is an approximate displacement corresponding to ϕ_i:

$$Sa' = [(\Sigma\, m_i\, \Delta_i^2) \,/\, (\Sigma\, m_i\, \Delta_i)^2]\; V \,/\, g \tag{4.6}$$

Similarly, the fundamental period, T, can be calculated using the following equation which can be derived using a Raleigh-Ritz type procedure:

$$T = 2\pi \sqrt{\frac{\Sigma\, m_i \Delta_i^2}{\Sigma\, P_i \Delta_i}} \tag{4.7}$$

As will be shown in the case study, the resulting capacity spectrum is plotted as a graph of the period, T, versus spectral acceleration, Sa'. Since higher modes of vibration are neglected in the analysis, an inherent assumption in the capacity spectrum method is that the fundamental mode of vibration dominates in the actual dynamic response.

SECTION 5
EXAMPLE CASE STUDY

5.1 2-D Frame: Inelastic Behavior and Connection Sensitivity Study

5.1.1 Design of PR Frame

The two story frame shown in Fig. 5-1 was designed based on the AISC-LRFD Specification [15] for gravity, wind, and earthquake loading. The wind load is based on a uniform pressure of 15 psf with a frame spacing of 25'.0", and the equivalent static earthquake forces are based on the UBC-88 [16] provisions for zone 2a. All members are assumed to be fully braced against out-of-plane displacements. The beam-column connections are modeled as top and seat angle with double web angle (TSAW) connections whose behavior is defined by the average curve (TSAW-AVE) using the parameters previously given in Table 2-2. In the initial analysis and design, the nominal connection strength, M_{cn}, was assumed to be 40% of the plastic moment, M_{pb}, of the adjacent beam. Once the member sizes were chosen, the connection angles were sized to provide a moment capacity of 0.4 M_{pb} using a design procedure described by Shen [13].

Design member forces were calculated based on a second-order analysis using CU-STAND. As shown in Fig. 5-1, beams and columns were discretized into 4 and 2 elements, respectively, and loads were applied at the nodes. Gravity and lateral loads were applied proportionally up to the full factored loads per the load combinations given by the Specification (LRFD Eqs. A4.2 to A4.5). In general, the gravity load combination controlled the beam sizes and the gravity/earthquake load combination controlled the column sizes. In the beam-column interaction equation design checks, the effective buckling length factors were calculated using the elastic eigenvalue buckling routine in CU-STAND. In this routine, the connection stiffness is taken as the initial tangent stiffness, K_e (see Fig. 2-1). The resulting effective length factors in the lower story were 1.65 and 0.85 for the exterior and interior columns, respectively.

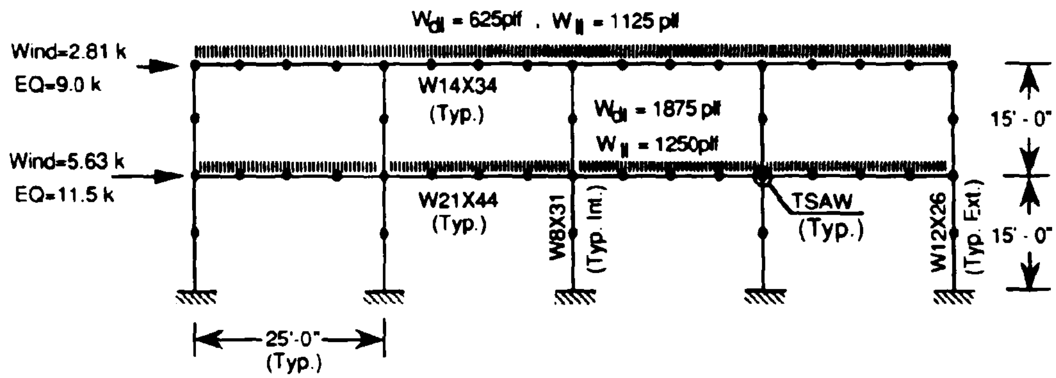

All Steel is A36

Loads Shown are Unfactored

<u>TSAW Connections:</u>

Top and Seat Angles: 4x4x3/4x6-1/2

Web Angles: 4x3-1/2x5/16x5-1/2

FIGURE 5-1 Two Dimensional Building Frame

As a serviceability check, the wind drift was calculated using the four load combinations with wind and earthquake load listed in Table 5-1. The load combination for checking the service drift includes the unfactored wind load (1.0 W) in combination with various amounts of gravity load. An additional service load combination, 1.0 DL + 0.4 LL + 0.5 W, which has been suggested by Ellingwood [17] is also included. According to Ellingwood, the combinations with full wind load are based on a 50 year recurrence interval, while that with 0.5 W is based on a 10 year recurrence interval. The calculated drifts are listed in Table 5-1, and in all cases the wind drift was less than H/400 = 0.9 inches. It is interesting to note that due to the nonlinear connection response, the calculated drift varied considerably (from 0.43 to 0.71 inches) depending on the amount of gravity load applied. Drift under a gravity load and earthquake load combination was equal to 1.34 inches corresponding to an index of H/270 which is less than the limit of H/200 specified in the UBC code for seismic loading.

TABLE 5-1 Roof Drift Under Service Loads

Load Combination	Drift (in)
1.0D + 1.0L + 1.0W	0.71
1.0D + 0.2L + 1.0W	0.53
1.0W	0.43
1.0D + 0.4L + 0.5W	0.29
1.0D + 0.2L + 1.0E	1.34

5.1.2 Inelastic Response

Using the member and connection sizes presented in the previous section, the limit state response of the frame was further evaluated using the second-order inelastic analysis feature of CU-STAND. The analyses were conducted for static loading and include geometric nonlinearities, semi-rigid connection response, and member plastification. In principle, this inelastic analysis can be used to satisfy the basic strength limit state design philosophy embodied in the following equation from the AISC LRFD Specification:

$$\gamma_i Q_i \leq \phi R_n \tag{5.1}$$

The left side of Eq. 5.1 represents the applied factored load effects and the right side is equal to the factored member resistances. Using a nonlinear inelastic analysis where most significant system and element destabilizing effects are included directly in the load effects (i.e., $\gamma_i Q_i$), the right side of Eq. 5-1 reduces to an expression for the factored (reduced) cross section capacity. In CU-STAND, the member resistance is given by a three dimensional yield surface which models elastic-plastic section response under axial load and biaxial bending [2]. In the analyses described below, the nominal yield surface in CU-STAND was reduced by the AISC-LRFD resistance factors for axial compression ϕ = 0.85 , tension ϕ = 0.9, and bending ϕ = 0.9 following a procedure suggested by Ziemian, et. al. [18].

<u>Gravity Loading</u>: For the inelastic gravity load analysis, the applied load was based on the following factored load combination (AISC-LRFD Eq. A4.2): $1.2\ D + 1.6\ L_F + 0.5\ L_R$. D is the total dead load, L_F is the live load on the floor beams, and L_R is the live load on the roof.

The overall response of the frame is described in Fig. 5-2. The moment diagram at the inelastic limit point is shown in Fig. 5-2a. Noted in this figure is the sequence of formation of the plastic hinges and the Applied Load Ratio (ALR) at which the hinges formed. (Note, throughout this report the magnitude of the applied load will be referred to as the Applied Load Ratio - ALR - which is the fraction of the factored load combination which has been applied to the structure.) As shown, the first hinges formed in the midspan of the beams in the end bents at a load equal to 1.06 times the full factored load. Subsequent hinges soon formed in the interior spans and then the columns until the structure failed at 1.38 times the factored load (ALR = 1.38) through a beam type collapse mechanism. The maximum connection rotation under the full factored load (ALR = 1.0) was 0.008 radian and this increased to 0.106 radian at the limit point (ALR = 1.38). Generally speaking, rotations greater than 0.050 radian are beyond the limit of most experimental data. Therefore, if the maximum connection rotations were limited in the analysis to 0.05 radian, the load ratio at the limit point would reduce from 1.38 to 1.14 which happens to be below the load at which hinges formed in the columns.

The inelastic redistribution of forces in the columns is evident through the force point traces in Fig. 5-2b where the normalized major axis bending and axial loads are plotted for the locations indicated. The dashed line shows the factored yield surface corresponding to the design (reduced full plastification) strength of the cross-section. As shown, the interior columns (sections C and D) pick up almost pure axial load until hinges (#1 and #2) form at the midspan of the floor beams. At this point the interior column begins to pick up moment and the exterior column picks up moment more rapidly. As the loading continues and the third hinge forms (Fig. 5-2a), the moment reverses at the base of the exterior column as the frame tends to collapse inwards. The fourth hinge forms at the top of the exterior columns (A) and under subsequent loading the member forces at section A are constrained to follow the yield surface. Thus, to pick up additional axial load, the moment at section A is redistributed elsewhere in the frame. Soon after hinge 4 forms, hinge 5 forms at section D followed in quick succession by hinges 6 and 7 whereupon the limit load is reached.

A plot of the Applied Load Ratio (ALR) versus the roof drift is shown in Fig. 5-2c. Since the frame is symmetric and does not tend to sidesway under symmetric loading, a second analysis was made in which an initial out-of-plumb of H/500 was introduced prior to application of the load. As shown, the initial imperfection results in a large increase in the lateral drift, but the overall strength, as measured by the applied load ratios at formation of the first hinge and limit point, does not change significantly. In fact, the inelastic limit point increased slightly for the case with imperfections (from 1.38 to 1.42), but this was associated with a 60% increase in the peak connection rotation (from 0.106 radian to 0.166 radian).

<u>Earthquake Loading</u>: The strength limit state for earthquake loading was evaluated based on the following factored load combination with gravity loads: 1.2 D + 0.5 L + 1.5E. Live loads are applied at both the floor and roof

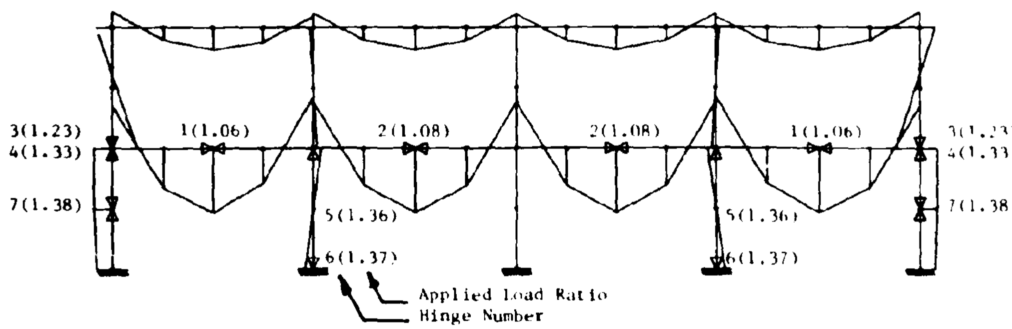

a) Bending Moments and Hinge Locations

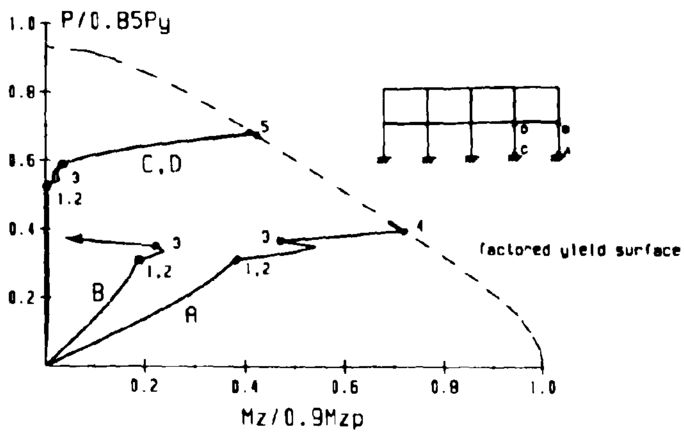

b) Force Point Traces

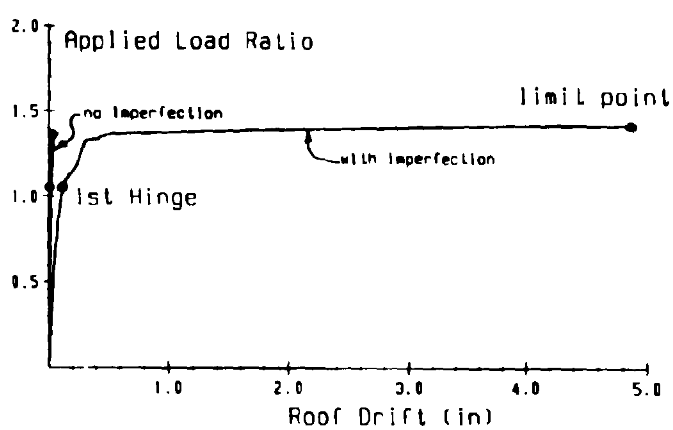

c) Applied Load Versus Roof Drift

FIGURE 5-2 Response Under Gravity Loading (1.2D + 1.6L_F + 0.5 L_R)

levels and E is the UBC equivalent static load. The overall response of the frame is described in Fig. 5-3. As shown in Fig. 5-3a, the relatively large lateral load caused hinges to form in the columns which resulted in the sidesway mechanism in the lower story. The first hinge formed in the leeward column at an applied load ratio of 1.02 and the limit point coincided with formation of the last hinge (# 7) at an applied load ratio of 1.19. The maximum connection rotation at the full factored load (ALR = 1.0) was 0.010 radian and at the limit point (ALR = 1.19) was 0.017 radian. The maximum connection rotation at the limit point was considerably smaller than in the gravity load case, and below the expected rotation capacity of 0.030 to 0.50 radians.

Force point traces for two of the lower story columns are shown in Fig. 5-3b and the overall load-deformation response of the frame is shown in Fig. 5-3c. For both columns shown in Fig. 5-3b, the yielding first occurs at the base of the columns (sections A and C). For loading beyond this point, the lower end of the columns redistribute bending moment to the top of the columns and adjacent columns to pick up additional axial loads. As indicated in Fig. 5-3c, the softening of the overall lateral stiffness due to the hinge formation occurs gradually until hinges (#1 to #4) form at the bases of all the columns where there is a noticeable kink in the load-deflection curve. Finally, at the limit point reached at 1.19 times the full factored load, the roof drift is 4.7 inches which corresponds to drift index of H/77.

Wind Loading: The strength limit state for wind loading was evaluated for the following load combination: 1.2 D + 0.5 L + 1.3 W. As noted previously, W is based on the equivalent static wind pressure. As shown in Fig. 5-4a, in this case the limit point was reached through a combination of hinges in the columns and beams. The first hinge formed at an applied load ratio of 1.50 and the limit load was reached at 1.67 times the full factored load. Unlike the previous case where the higher lateral loading dominated the response, in this case the limit load response was due to a combination of gravity and lateral effects. This is evident from the force point traces in Fig. 5-4b where, unlike the traces under earthquake load (Fig. 5-3b), the moments of the top of the columns (sections B and D) did not increase dramatically after the hinges (#5 to 9)formed at the base of the columns

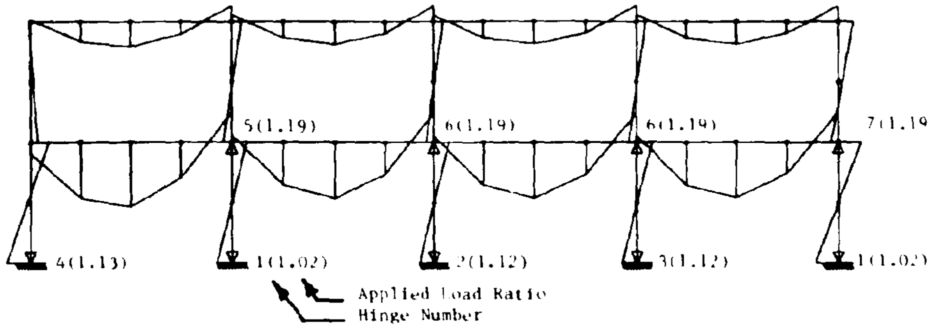

a) Bending Moments and Hinge Locations

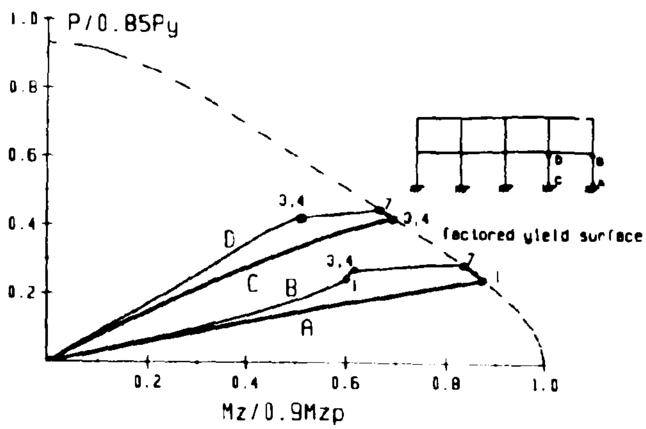

b) Force Point Traces

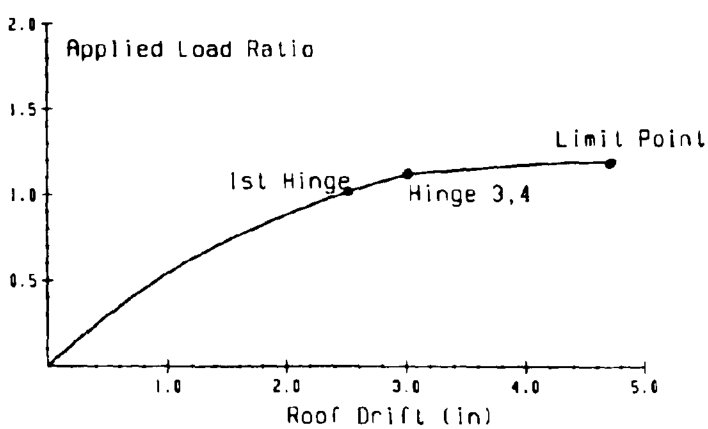

c) Applied Load Versus Roof Drift

FIGURE 5-3 Response Under Gravity Plus Earthquake Loading (1.2D + 0.5L + 1.5E)

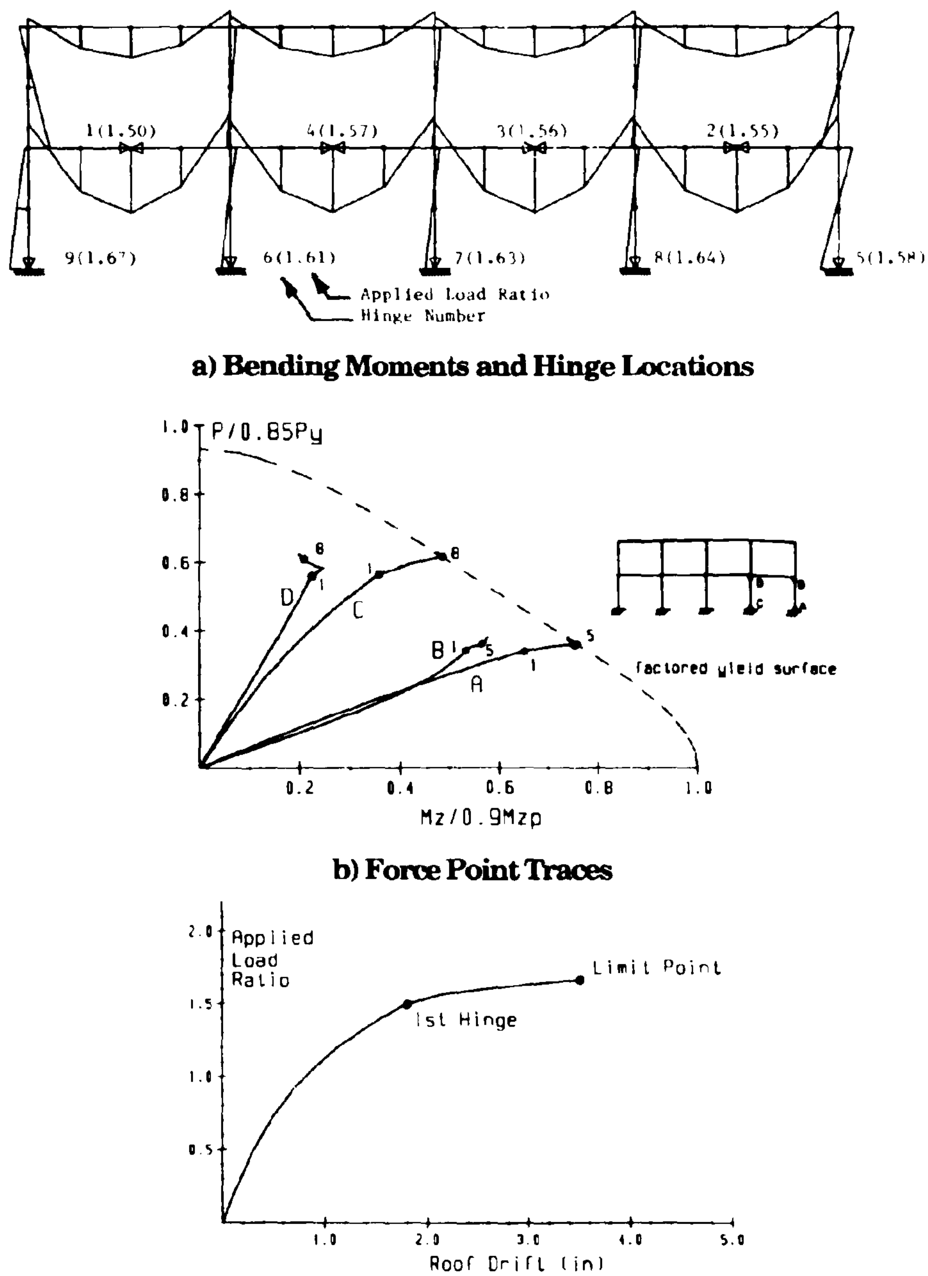

a) Bending Moments and Hinge Locations

b) Force Point Traces

c) Applied Load Versus Roof Drift

FIGURE 5-4 Response Under Gravity Plus Wind Loading (1.2D + 0.5L + 1.3W)

(sections A and C). The overall load-deformation response of the frame is shown in Fig. 5-3c where the roof drift at the limit point was 3.5 inches which corresponds to a drift index of H/103.

Non-proportional Loading: The inelastic response of the frame under non-proportional gravity and lateral loading was also investigated and the resulting load-deformation plots are shown in Fig. 5-5. In the two nonproportional analyses, gravity loads were applied up to the full factored load (1.2 D + 0.5 L), and then the factored lateral loads (1.5 E and 1.3W, respectively) were increased until the inelastic limit point was reached. In both cases, the nonproportional loading resulted in a higher limit point than in the proportional loading case. For the earthquake loading, the increase was 15% (from 1.19 to 1.37) and for the wind loading, the increase was 125% (from 1.67 to 3.76). Note that a direct comparison between the proportional and non-proportional load case beyond an applied load ratio of 1.0 is somewhat misleading because in the nonproportional case the applied load ratio for the gravity load is held constant at 1.0. However, the nonproportional load case gives a better indication of the limit state associated with increasing intensity of lateral loads. As will be discussed, the capacity spectrum analysis is based on nonproportional gravity and earthquake loading.

5.1.3 Sensitivity to Connection Parameters

To evaluate the sensitivity of the overall frame response to the variation in connection response parameters (see Section 2) several analyses were run using different connection parameters. In the first set of analyses, the effect of varying the assumed shape of the connection curve is evaluated by modifying the parameters M_0', K_e', K_p', and n (see Eq. 2.5). In the second set of analyses, the effect of varying the assumed strength of the connection, M_{cn}, is investigated.

Effect of Connection Model Shape: As discussed in Section 2, the variability of the shape of the assumed connection response model for TSAW connections is bounded by the curves TSAW-UPPER and TSAW-LOWER which represent a variation of two standard deviations from the mean curve

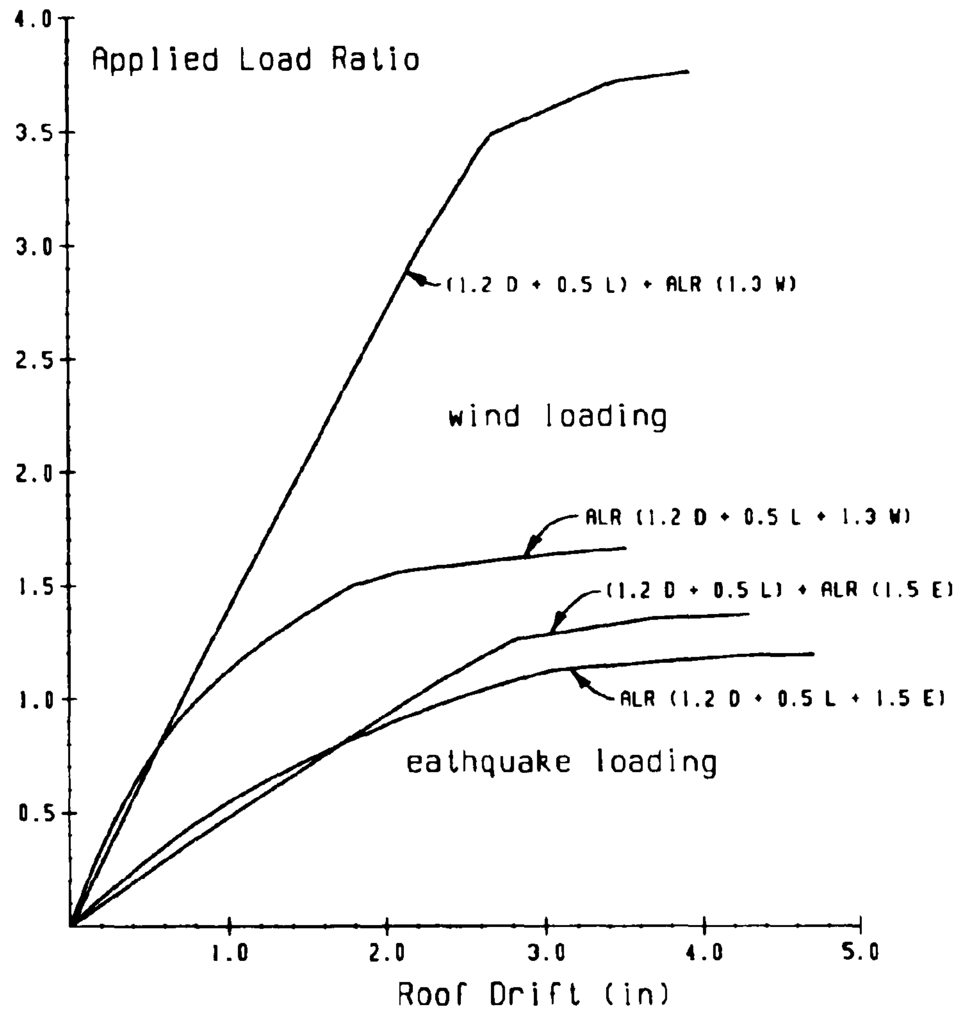

FIGURE 5-5 Comparison of Response Under Proportional and Nonproportional Loading for Gravity and Lateral Loads

TSAW-AVE (see Fig. 2-4b). Also, the shape of the TSAW-AVE curve can be approximated by the DESIGN curve which is an average model representative of all connection types (see Fig. 2-6). The curve parameters for the TSAW-AVE, TSAW-LOWER, and TSAW-UPPER models are given in Table 2-2 and values for the DESIGN curve are given in Section 2.3. In the following discussion, the effect of the assumed shape of the response curve is assessed by comparing results from four sets of inelastic analyses in which the curve parameters (M_o', K_e', K_p', and n) were varied. For all cases, the assumed connection strength was kept constant with $M_{cn} = 0.4$ M_{pb}.

A summary of the applied load ratio at the occurrence of the first plastic hinge and at the limit point is presented in Table 5-2. The results indicate practically no differences in the calculated load ratios between the different cases. Results for the TSAW-AVE and DESIGN curve are within 1%, and results for all of the curves are within 5%. Comparisons between calculated maximum connection rotations and deformations are summarized in Tables 5-3 to 5-5 where again there is no significant difference in the response.

Effect of Connection Strength. Since the connection response curve is normalized by the nominal connection strength, the assumed connection strength has an effect on both the stiffness and strength of the moment-rotation behavior of the connection model. To investigate the effect of varying the strength, three sets of analyses are compared where in each case, M_{cn} is set to 0.3 M_{pb}, 0.4 M_{pb}, and 0.5 M_{pb}, respectively. The assumed variation in strength of 25% from 0.4 M_{pb} is approximately equal to one standard deviation between calculated and measured values of connection strengths for TSAW connections based on data from 17 tests [13].

As shown in Table 5-6, an increase in connection strength generally increased the applied load ratio at the first hinge and limit point, although the relative change in applied load ratio was less than the change in connection strength. For example, while the variation in connection strength was ±25% compared to the case with $M_{cn} = 0.4$ M_{pb}, the variation in load ratios was within -8% to +6%. Also, there tended to be a larger variation in

TABLE 5-2 Applied Load Ratios for Frames with TSAW Connections (M_{cn} = 0.4 M_{pb})

Criteria	Loading	Applied Load Ratios			
		Upper	Ave	Lower	Design
1st Hinge	1.2D + 1.6 L_F + 0.5 L_R	1.09	1.06	1.03	1.05
	1.2D + 0.5L +1.3W	1.52	1.50	1.47	1.49
	1.2D + 0.5L + 1.5E	1.02	1.02	1.03	1.02
Limit Point	1.2D + 1.6L_F + 0.5L_R	1.31	1.38	1.44	1.33
	1.2D + 0.5L + 1.3W	1.62	1.67	1.70	1.64
	1.2D + 0.5L + 1.5E	1.20	1.19	1.19	1.19

TABLE 5-3 Maximum Connection Rotations for Frames With TSAW Connections (M_{cn} = 0.4 M_{pb})

Criteria	Loading	Maximum Rotation (10^{-3} radian)			
		Upper	Ave	Lower	Design
Service	1.0D + 1.0L	5.6	6.6	7.5	7.0
	1.0D + 0.2L+1.0W	3.1	3.9	4.8	4.3
Full Factored	1.2D + 1.6L_F + 0.5L_R	7.6	8.3	9.0	8.6
	1.2D + 0.5L + 1.3W	5.5	6.2	7.0	6.5
	1.2D + 0.5L + 1.5E	9.4	9.9	10.4	10.0
Limit Point	1.2D + 1.6L_F + 0.5L_R	114	106	105	112
	1.2D + 0.5L + 1.3W	36	42	41	40
	1.2D + 0.5L + 1.5E	17	17	17	17

TABLE 5-4 Maximum Floor Beam Deflections for Frames with TSAW Connections (M_{cn}= 0.4 M_{pb})

Criteria	Loading	Deflection (inch)			
		Upper	Ave	Lower	Design
Service	1.0D + 1.0L	0.66	0.72	0.77	0.74
Full Factored	1.2D + 1.6L_F + 0.5L_R	0.97	1.03	1.08	1.05
Limit Point	1.2D + 1.6L_F + 0.5L_R	17.20	16.47	16.80	16.88

TABLE 5-5. Roof Drift for Frames with TSAW Connections (M_{cn}= 0.4 M_{pb})

Criteria	Loading	Drift (inch)			
		Upper	Ave	Lower	Design
Service	1.0D + 0.2L + 1.0W	0.49	0.53	0.57	0.55
Full Factored	1.2D + 0.5L + 1.3W	0.77	0.82	0.84	0.82
	1.2D + 0.5L + 1.5E	2.37	2.44	2.84	2.45
Limit Point	1.2D + 0.5L + 1.3W	3.77	3.51	3.33	3.58
	1.2D + 0.5L + 1.5E	4.76	4.71	4.75	4.75

TABLE 5-6. Applied Load Ratios for Frames with TSAW Connections: Effect of Connection Strength

Criteria	Loading	Applied Load Ratios		
		M_{cn}=0.3M_{pb}	M_{cn}=0.4M_{pb}	M_{cn}=0.5M_{pb}
1st Hinge	1.2D + 1.6 L_F + 0.5 L_R	0.99	1.05	1.10
	1.2D + 0.5L +1.3W	1.41	1.49	1.56
	1.2D + 0.5L + 1.5E	1.00	1.02	1.04
Limit Point	1.2D + 1.6L_F + 0.5L_R	1.22	1.33	1.41
	1.2D + 0.5L + 1.3W	1.54	1.64	1.73
	1.2D + 0.5L + 1.5E	1.17	1.19	1.21

applied load ratios for the gravity load only and gravity plus wind load combinations where hinges formed in the beams. The variation for the gravity plus earthquake load case was not as large. This trend is also apparent in the load-deflection response curves for the two lateral load cases which are shown in Figs. 5-6a and 5-6b. In both cases there were differences in calculated deflections, but significant differences in the strength limit point did not occur under the earthquake loading.

Comparisons of the maximum connection rotations and deflections for the three assumed connection strengths are shown in Tables 5-7 to 5-9. In general, the connection rotations and deflections decreased with increasing connection strength, and the percentage change was greater between the cases with M_{cn} = 0.3 to 0.4 M_{pb} than between the cases with M_{cn} = 0.4 to 0.5 M_{pb}. For the cases with M_{cn} = 0.3 M_{pb}, the connection deformations varied up to +35% and the deflections varied up to +31% compared to those for M_{cn}

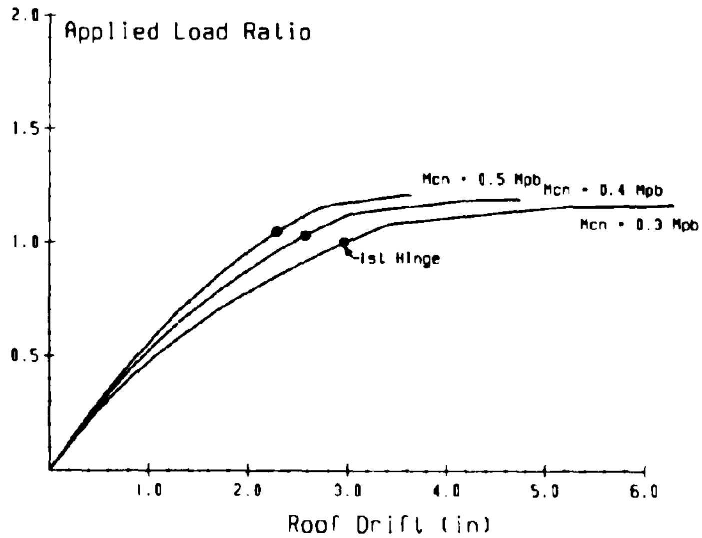

a) Gravity Plus Earthquake Loading (1.2D + 0.5L + 1.5E)

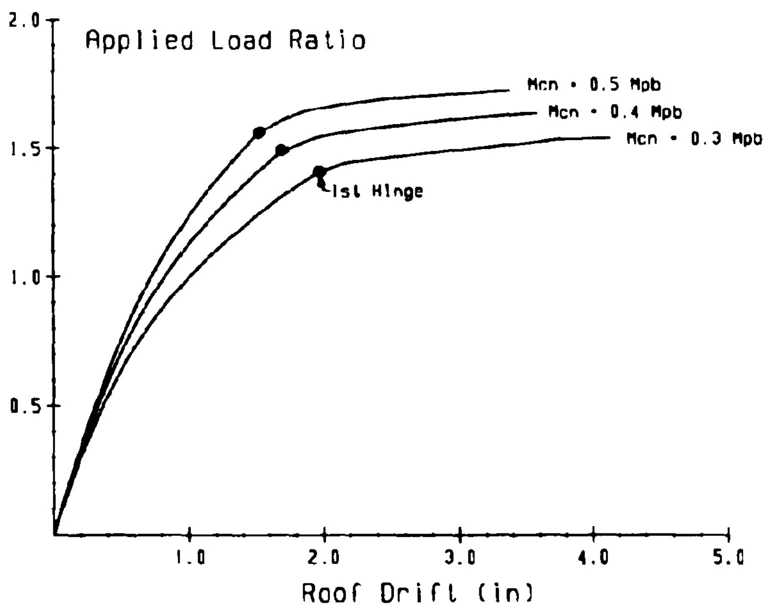

b) Gravity Plus Wind Loading (1.2D + 0.5L + 1.3W)

FIGURE 5.6 Effect of Connection Strength on Response

TABLE 5-7. Maximum Connection Rotations for Frames With TSAW Connections: Effect of Connection Strength

Criteria	Loading	Maximum Rotations (10^{-3} radian)		
		$M_{cn}=0.3M_{pb}$	$M_{cn}=0.4M_{pb}$	$M_{cn}=0.5M_{pb}$
Service	1.0D + 1.0L	8.5	7.0	5.8
	1.0D + 0.2L +1.0W	5.3	4.3	3.6
Full Factored	1.2D + 1.6L_F + 0.5L_R	11.1	8.6	7.5
	1.2D + 0.5L + 1.3W	8.1	6.5	5.4
	1.2D + 0.5L + 1.5E	13.5	10.0	7.4

TABLE 5-8. Maximum Floor Beam Deflection for Frames with TSAW Connections: Effect of Connection Strength

Criteria	Loading	Deflection (inch)		
		$M_{cn}=0.3M_{pb}$	$M_{cn}=0.4M_{pb}$	$M_{cn}=0.5M_{pb}$
Service	1.0D + 1.0L	0.81	0.74	0.69
Full Factored	1.2D + 1.6L_F + 0.5L_R	1.38	1.05	0.98

TABLE 5-9. Roof Drift for Frames with TSAW Connections: Effect of Connection Strength

Criteria	Loading	Drift (inch)		
		$M_{cn}=0.3M_{pb}$	$M_{cn}=0.4M_{pb}$	$M_{cn}=0.5M_{pb}$
Service	1.0D + 1.2L + 1.0 W	0.64	0.55	0.50
Full Factored	1.2D + 0.5L + 1.3W	1.01	0.82	0.73
	1.2D + 0.5L + 1.5E	2.97	2.45	2.14

= 0.4 M_{pb}. For the cases with M_{cn} = 0.5 M_{pb}, the connection deformations varied up to -25% and the deflections varied up to -13% compared to those for M_{cn} = 0.4 M_{pb}. Presumably, there were smaller variations between the case with higher connection strength because, as the connection becomes stiffer, the overall structural flexibility becomes less a function of the connection stiffness and more a function of the overall frame geometry and member properties.

5.2 2-D Frame: Inelastic Seismic Response

5.2.1 Frame Designs

The two story frame described in Section 5.1 is used in this section to demonstrate the capacity spectrum method for evaluating inelastic response under earthquake loading. To investigate the effect of connection restraint, four separate frame designs are considered. In three designs, the connections were modeled as semi-rigid with strengths of M_{cn} = 0.1 M_{pb}, 0.4 M_{pb}, and 1.2 M_{pb}, respectively. Generally speaking, connections with: (1) 0.1 M_{pb} correspond to details with light weight top and seat angles, (2) 0.4 M_{pb} correspond to details with medium weight top and seat angles with web angles, and (3) 1.2 M_{pb} correspond to thick stiffened end plate details. In all cases, the DESIGN curve parameters (K_e' = 200, K_p' = 4, M_o' = 1.0, n = 1.4) were used to define the shape of the connection response curve. In the fourth frame, the connections were assumed to be rigid.

Each of the four frames was designed to meet the AISC-LRFD provisions as described previously in Section 5.1.1 and the resulting member sizes are given in Table 5-10. The total weight of structural steel is also listed in Table 5-10. All members were designed using A36 (F_y = 36 ksi) steel.

TABLE 5-10 Member Sizes and Total Weight of Structural Steel for Seismic Response Study.

Member	M_{cn} = 0.1 M_{pb}	M_{cn} = 0.4 M_{pb}	M_{cn} = 1.2 M_{pb}	Rigid
Interior Columns	W8x35	W8x31	W8x31	W8x31
Exterior Columns	W12x30	W12x26	W12x30	W12x30
Floor Girders	W21x57	W21x44	W18x44	W21x44
Roof Girders	W18x35	W14x34	W16x26	W16x31
Steel.Weight (kips)	14.15	12.15	12.59	12.09

Inelastic analyses under proportioned loading were conducted for all cases under various loading conditions and the results are summarized in Tables 5-11 to 5-14. Variations in the applied load ratios shown in Table 5-11 appear to be due to the fact that various members in the different frames were slightly overdesigned by different amounts. One exception to this is that the frame with rigid connections consistently carried higher loads at the limit point. As indicated in Tables 5-12 to 5-14, the main difference in behavior between the frames was that connection rotations and deformations were larger in the frames with less connection rigidity. For example, under the full factored and earthquake loadings roof drift was roughly 30%, 80%, and 200% greater for the frames with EEPS, TSAW, and TSA connections (respectively) compared to the rigid frame.

5.2.2 Capacity Spectrum Analysis

The capacity spectrum analysis was made using nonproportional loading where the full factored gravity load is first applied to the frame. For combination with earthquake loads, the factored gravity load combination was 1.2D + 0.5L. Once the gravity load was applied, the factored earthquake loading was increased until the inelastic limit point was reached. The resulting load-deformation response for each of the four frames is shown in Fig. 5-7. Note that, in this case under nonproportional loading, the TSA frame reached a higher load than the TSAW frame. This is due to the fact that the TSA frame was designed with larger columns than the TSAW frame, and as discussed previously, under earthquake loading the frames fail by a story mechanism where hinges form in the columns (see Fig. 5-3a).

The capacity spectrum curves for each of the frames are shown in Fig. 5-8 along with design spectrum (NBK) curves proposed by Newmark, et. al. [19]. The curves are based on a peak ground acceleration of 0.15g to correspond to the UBC code based loading for Zone 2a. The NBK curves with 1% and 10% damping were chosen to give a representative measure of the frame response in the elastic range (1% damping), and at the inelastic limit point (10% damping). For calculating the period and spectral acceleration, the mass was based on the total dead load plus 20% of the live load.

TABLE 5-11 Applied Load Ratios for Frames Designed with TSA, TSAW, EEPS and Rigid Connections

Criteria	Loading	Applied Load Ratios			
		TSA (.1 M_{pb})	TSAW (.4 M_{pb})	EEPS (1.2 Mpb)	Rigid
1st Hinge	1.2D + 1.6 L_F + 0.5 L_R	1.15	1.05	1.13	1.09
	1.2D + 0.5L +1.3W	1.64	1.49	1.62	1.49
	1.2D + 0.5L + 1.5E	1.05	1.02	1.12	1.16
Limit Point	1.2D + 1.6L_F + 0.5L_R	1.31	1.33	1.32	1.61
	1.2D + 0.5L + 1.3W	1.68	1.64	1.79	1.97
	1.2D + 0.5L + 1.5E	1.17	1.19	1.29	1.32

TABLE 5-12 Maximum Connection Rotations for Frames Designed with TSA, TSAW, EEPS, and Rigid Connections

Criteria	Loading	Maximum Rotation (10^{-3} radian)			
		TSA (.1 M_{pb})	TSAW (.4 M_{pb})	EEPS (1.2 Mpb)	Rigid
Service	1.0D + 1.0L	8.4	7.0	3.1	---
	1.0D + 0.2L +1.0W	6.5	4.3	2.1	---
Full Factored	1.2D + 1.6L_F + 0.5L_R	9.3	8.6	4.7	---
	1.2D + 0.5L + 1.3W	9.8	6.5	3.1	---
	1.2D + 0.5L + 1.5E	18.4	10.6	3.9	---
Limit Point	1.2D + 1.6L_F + 0.5L_R	133.0	112.0	7.2	---
	1.2D + 0.5L + 1.3W	215.0	40.0	7.2	---
	1.2D + 0.5L + 1.5E	36.8	17.0	6.1	---

TABLE 5-13 Maximum Floor Beam Deflections for Frames Designed with TSA, TSAW, EEPS, and Rigid Connections

Criteria	Loading	Deflection (inch)			
		TSA (.1 M_{pb})	TSAW (.4 M_{ph})	EEPS (1.2 Mpb)	Rigid
Service	1.0D + 1.0L	0.72	0.74	0.68	0.25
Full Factored	1.2D + 1.6L_F + 0.5L_R	0.98	1.05	0.95	0.56
Limit	1.2D + 1.6L_F + 0.5L_R	19.30	16.88	30.89	40.43

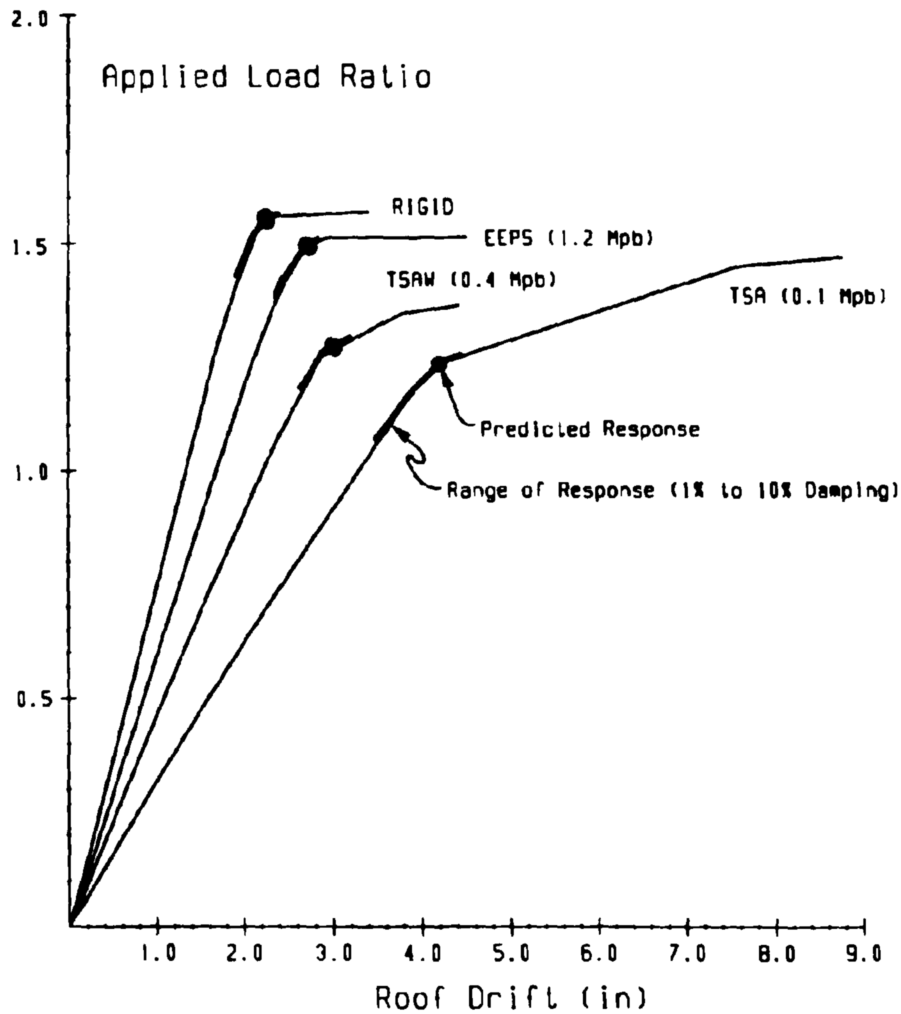

FIGURE 5-7 Applied Load Versus Drift Under Nonproportional Gravity Plus Earthquake Loading ((1.2D + 0.5L) + ALR (1.5E)

TABLE 5-14 Roof Drift for Frames Designed with TSA, TSAW, EEPS, and Rigid Connections

Criteria	Loading	Drift (inch)			
		TSA (.1 M_{pb})	TSAW (.4 M_{pb})	EEPS (1.2 Mpb)	Rigid
Service	1.0D + 0.2L + 1.0W	0.87	0.55	0.44	0.35
Full Factored	1.2D + 0.5L + 1.3W	1.43	0.82	0.60	0.47
	1.2D + 0.5L + 1.5E	3.90	2.45	1.69	1.33
Limit	1.2D + 0.5L + 1.3W	4.34	3.58	3.07	2.15
	1.2D + 0.5L+ 1.5E	9.95	4.75	2.67	2.17

As expected, the initial period (i.e., when Sa' = 0) was smallest for the RIGID frame and largest for the TSA frame. Also, since the first hinges formed at a higher load ratio, the stiffness of the RIGID and EEPS frame degraded at a larger value of spectral acceleration. However, the fundamental period at the limit point was nearly the same in all cases.

The NBK design spectra can be viewed of as the required strength (or strength demand) on a system with a given fundamental period and level of damping. For the frames considered, the transition curve (shown dashed) between 1% and 10% damping is an approximation for the demand on the system as it undergoes inelastic deformation. Point **a** is the point on the 1% (elastic) demand curve corresponding to the initial period of the structure. Point **b** is the point on the 10% (inelastic limit) demand curve corresponding to the period of the structure at its inelastic limit point (the intersection point for pt. **b** is based on the maximum period on the capacity spectrum curve which relates to the inelastic limit point from Fig. 5-7). Theoretically, the transition curve is different for each structure (since the initial and final periods vary), but in this case the differences are small and a single average transition curve is used.

The intersection of the capacity spectrum and transition demand spectrum curves gives the predicted response of each structure. The point at which the curves intersect can be related back to the load vs. deformation curve as shown in Fig. 5-7. Also included in Fig. 5-7 is an indication of the response range which corresponds to the intersection of the capacity spectrum curve with the 1% and 10% NBK curves.

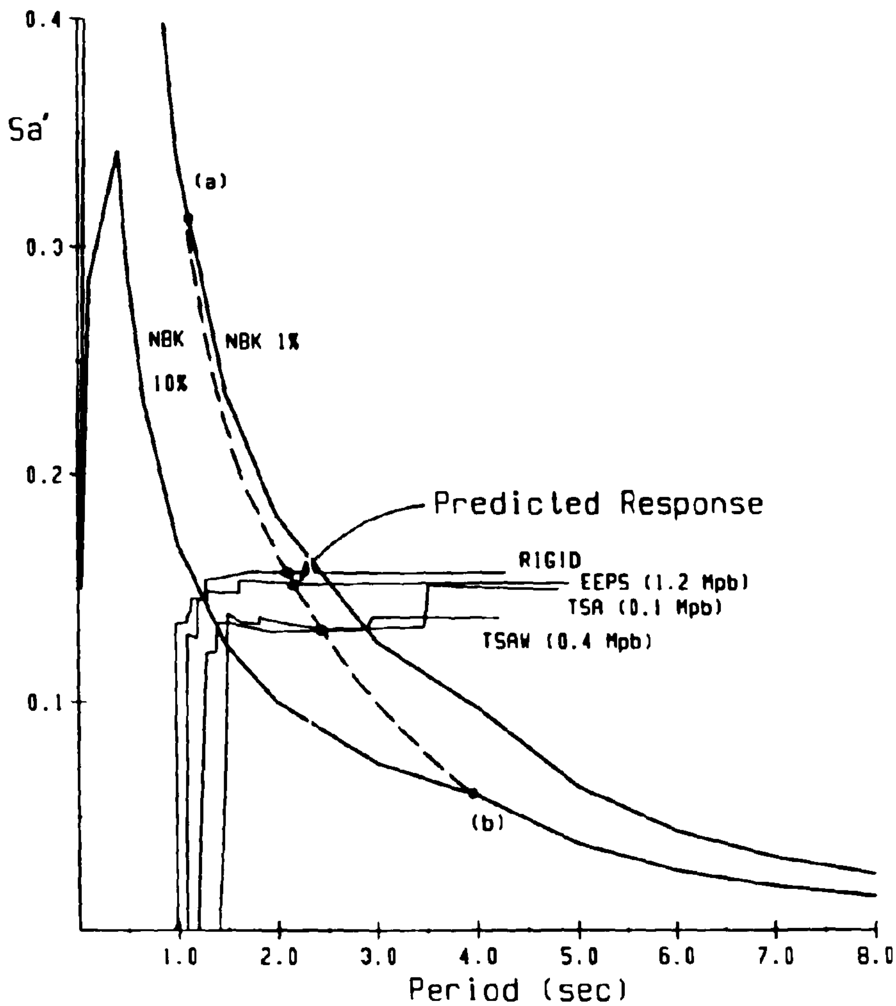

FIGURE 5-8 Capacity Spectra Versus NBK Design Spectra

A summary of several measures for the predicted response is given in Table 5-15. Insofar as basic strength is concerned, the seismic resistance of all the frames is comparable. Due to their greater stiffness, the EEPS and RIGID frames resisted higher base shears, but as shown in Figs. 5-7 and 5-8, in all cases the predicted response was below the inelastic limit point. The connection rotations were larger for the TSA and TSAW frames, but the maximum rotations were still relatively modest. Assuming the joints are properly detailed to provide a ductile response, most connections of the types considered have rotation capacities of at least 0.030 to 0.050 radians whereas the peak rotation demand was 0.019 radians (for the TSA frame). Finally, the main significant differences in response were in the lateral drifts which was 40% greater in the TSA frame and 10% and 25% less in the EEPS and rigid frame (respectively) compared to the TSAW frame.

TABLE 5-15 Comparison of Response Measures for Frames with Different Connection Strengths

Response Parameter	TSA	TSAW	EEPS	RIGID
Base Shear (kips)	38.1	39.0	45.9	47.8
Max. Conn. Rotation (rad x 10^{-3}	19	12	5	----
1st Floor Drift (in)	1.95	1.67	1.61	1.45
Roof Drift (in)	4.24	3.02	2.71	2.25

The roof drifts predicted by the capacity spectrum analyses are compared to those calculated using the 2nd-order static analyses at full factored loading in Fig. 5-9. In all cases, the drifts calculated by the capacity spectrum are greater (+ 9% to + 69%) than calculated under the equivalent static earthquake load. In additon, the difference between the two analyses is larger for the frames with greater connection rigidity.

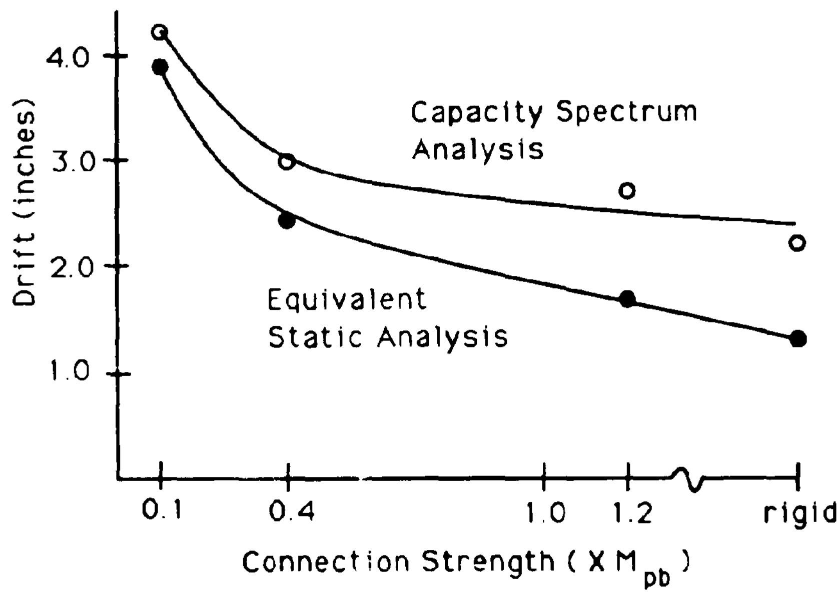

FIGURE 5-9 Comparison of Drifts Under Factored Earthquake Loading

SECTION 6
SUMMARY AND CONCLUSIONS

The main purpose of the reported research is to provide an analysis and design tool for investigating the effect of semi-rigid connections on the behavior and design of steel frames subjected to static or quasidynamic loading. There are four main components included in the current work: (1) adoption and development of a connection model suitable for use in analysis and design; (2) modeling of the connection element in finite element analysis; (3) computer implementation of the semi-rigid connection model and the capacity spectrum method; and (4) use of the system to investigate the limit state response of a low-rise frame with semi-rigid connections.

A four parameter equation is used to model the nonlinear moment-rotation behavior in the overall frame analysis. In the computer implementation, two methods are provided for determining the parameters for the model. The first method uses a built-in curve fitting routine to fit the model to a user-defined set of moment-rotation data. This feature has been demonstrated to provide good results when used to fit the model to experimental data. The second method for assigning parameters is by direct user input. In conjunction with this method, suggested values of normalized parameters are based on calibration to existing test data for several types of connections. A set of normalized parameters based on the average response of several different types of connections is also proposed.

The "zero-length" connection elements are implemented in finite element analysis to model connection flexibility for both major- and minor-axis rotational degrees-of-freedom. In the finite element formulation, additional local degrees-of-freedom associated with the flexibility at connections are introduced into the global solution system. Conventional element transformation matrices are modified for the beam-column elements connected with semi-rigid connections. A key advantage of the approach used is that the existing nonlinear model for the beam-column elements is unaffected. The approach presented simplifies the computer implementation of connection flexibility for three-dimensional nonlinear analysis and facilitates further modification of the connection model.

The semi-rigid connections are implemented in the existing interactive-graphics analysis and design system for three-dimensional structures, CU-STAND. The tool developed is capable of analyses considering both geometric and material nonlinearities, and semi-automated member redesign based on a subset of the AISC LRFD Specification. In addition, the advantages of interactive computer graphics are utilized in controlling the analysis, monitoring the structural response, defining and editing the connection model, and attaching connections to the structure. To provide a means for estimating the seismic performance of steel frames with semi-rigid connections, the Capacity Spectrum method is also implemented in CU-STAND.

A case study for a two-story planar frame with partially restrained connections is used to: (1) investigate the inelastic limit state response, (2) evaluate the sensitivity of overall frame behavior to variations in the connection behavior, and (3) use the capacity spectrum method to predict the inelastic response under seismic loading. The inelastic limit state was investigated for a frame with top and seat and double web angle (TSAW) connections with a moment capacity of 40% of the plastic moment of the connected beams. The frame was designed using the AISC-LRFD code provisions considering gravity, wind, and earthquake (UBC - Zone 2a) loading. Based on the results of a second-order inelastic analysis, the inelastic limit point was reached at load ratios roughly 20% to 30% greater than the full factored loads for the controlling load cases. In general, the connection rotations were not excessive; under full factored load they were less than 0.01 radians and at the limit point they were usually less than 0.05 radians. One exception to this was under pure gravity loading where the peak rotations increase up to 0.10 radians where beam mechanisms formed. Based on test data reported in the literature, connection rotation capacities of 0.03 to 0.05 radians seem to be quite common. Under service loads the drift indices were less than H/500 for wind loading and H/270 for earthquake loading. Under full factored loads the drift increases to H/430 for wind and H/130 for earthquake and at the limit point increased further to H/95 and H/75, respectively. The large drifts at the limit point demonstrate the importance (even for low-rise structures) of nonlinear geometric effects on the inelastic limit state behavior. Finally, based on the nonlinear analysis, information on the inelastic force redistribution at the limit point is provided.

Comparison of the overall response for frames with varying connection properties indicates that (1) there is no significant effect due to statistical variations in the normalized connection model parameters, but (2) there is a significant effect due to variations in the assumed connection strength. In the sensitivity study, comparisons of inelastic limit points, deformations, and hinge formations were made for frames with top and seat angle with double web angle connections. In the first comparison, the normalized parameters (K_c', K_p', M_0' and n) were varied to reflect a statistical variation of ±2 standard deviations from the average connection response curve. In the second comparison, the connection strengths were varied between 0.3, 0.4, and 0.5 times the plastic moments of the connected beams; this reflected a variation in strength of ± 25% from the case with $M_{cn} = 0.4\ M_{pb}$. Changes in the inelastic limit points were less than ± 8% which indicates that the overall strength was not very sensitive to the connection strength. On the other hand, changes in the deformations ranged up to ±30% which reflects a strong correlation with the connection strength, M_{cn}, used in the moment-rotation model.

The inelastic response under equivalent static seismic loads was evaluated for several frames with varying connection rigidity based on code specified forces and a capacity spectrum analysis. In general, the capacity spectrum analysis indicated more severe loading than the code based equivalent static forces in terms of maximum base shear and deformations. Also, the difference in predicted response was larger for the frames with greater connection rigidity. In all cases, however, the frames which were designed for code forces exhibited adequate strength based on the inelastic capacity spectrum analysis.

The results of the low-rise case study provide information on a certain geometry and frame configuration which may or may not be applicable to other frames with partially restrained connections. As noted previously, however, the main purpose of this report is not to present behavior information which covers a wide variety of structures. Rather, the purpose herein is to describe and demonstrate a computer-aided system which can be used to investigate the inelastic response of most steel building frames with partially restrained connections under static or equivalent static earthquake loading.

SECTION 7
REFERENCES

1. McGuire, W., Deierlein, G. G., Sooi, T. K., Zhao, Y. T., Illustrated Primer to CU-PREPF, CU-STAND, and CU-QUAND, Structural Engineering Report No. 89-12, School of Civil & Environmental Engineering, Cornell University, Ithaca, NY, October 1989.

2. Hsieh, S. H., Deierlein, G. G., McGuire, W., Abel, J. F., Technical Manual for CU-STAND, Structural Engineering, Report No. 89-13, School of Civil and Environmental Engineering, Cornell University, Ithaca, NY, October 1989.

3. Zhao, Y. T., Deierlein, G. G., Abel, J. F., McGuire, W., Technical Manual for CU-QUAND, Structural Engineering Report No. 89-14, School of Civil and Environmental Engineering, Ithaca, NY, October 1989.

4. Hsieh, S. H., Zhao, Y. T., Deierlein, G. G., Abel, J. F., Programmers Manual for CU-PREPF, CU-STAND, and CU-QUAND, Structural Engineering Report No. 89-15, School of Civil & Environmental Engineering, Ithaca, NY, December 1989.

5. Freeman, S. A., "Prediction of Response of Concrete Buildings to Severe Earthquake Motion," Douglas McHenry International Symposium on Concrete and Concrete Structures, SP-55, American Concrete Institute, Detroit, Michigan, 1978, pp. 589-605.

6. Chrysostomou, C. Z., Gergely, P., Abel, J. F., "Preliminary Studies of the Effect of Degrading Infill Walls on the Nonlinear Seismic Response of Steel Frames." Tech. Report NCEER-88-0046, National Center for Earthquake Engrg. Research, Buffalo, NY 1988.

7. Connections Bibliography, Structural Stability Research Council, Task Group 25, Glenn Morris, editor, September 1986..

8. Richard, R. M., Abbott, B. J., "Versatile Elastic-Plastic Stress-Strain Formula, "Journal of the Engrg. Mechanics Div., ASCE, Vol. 101, EM4, August 1975, pp. 511-515.

9. Chen, W. F., Kishi, N., "Semi-rigid Steel Beam-to-Column Connections: Data Base and Modelling," J. Struct. Engrg., 115, 1989, pp. 105-119.

10. Hsieh, S. H., "Analysis of Three-Dimensional Frames with Semi-Rigid Connections," M. S. Thesis, School of Civil and Environmental Engineering, Cornell University, January 1990.

11. Kishi, N. Chen, W. F., "Data Base on Steel Beam-to-Column Connections," CE-STR-86-26, School of Civil Engineering, Purdue University, West Lafayette, IN, 1986.

12. Goverdham, A. V., "A Collection of Experimental Moment-Rotation Curves and Evaluation of Predicting Equations for Semi-Rigid Connections," M.S. Thesis, Department of Civil Engineering, Vanderbilt University, Nashville, TN, 1983.

13. Shen, Y. J., "Computer-Aided Design of Steel Frames with Partially Restrained Connections," M.S. Thesis, School of Civil and Environmental Engineering, Cornell University, August 1990.

14. McGuire, W., Gallagher, R. H., Matrix Structural Analysis, John Wiley and Sons, New York, 1979.

15. American Institute of Steel Construction, Load and Resistance Factor Design Specification for Structural Steel Buildings, First Edition, AISC, Chicago, IL, 1986.

16. International Conference of Building Officials, Uniform Building Code, 1988 Edition, ICBO, Whittier, CA, 1988.

17. Ellingwood, B., "Serviceability Guidelines for Steel Structures," Engineering Journal, AISC, Vol. 26, No. 1, 1989, pp. 1-8.

18. Ziemian, R. D., White, D. W., Deierlein, G. G., McGuire, W., "One Approach to Inelastic Analysis and Design," Proceedings of the 1990 National Steel Construction Conference, AISC, Chicago, 1990, pp. 19.1 to 19.19.

19. Newmark, N. M., Blum, J. A., Hapur, K. K., "Seismic Design Spectra for Nuclear Power Plants," Journal of the Power Division, ASCE, Vol. 99, No. PO2, Proc. Paper 10142, 1973, pp. 287-303.

APPENDIX A

SEMI-RIGID CONNECTION DATA

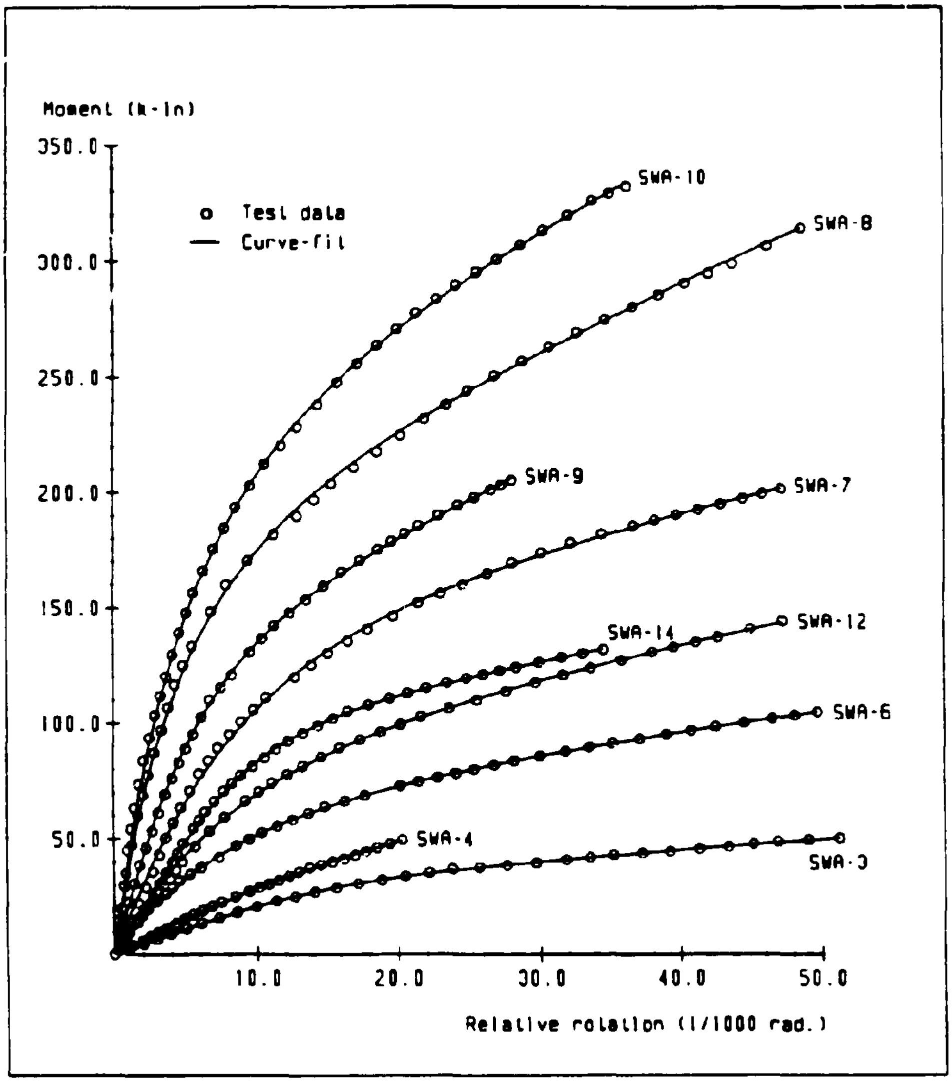

FIGURE A-1 Comparison Between Curve-fitting and Experimental Results for SWA Connections

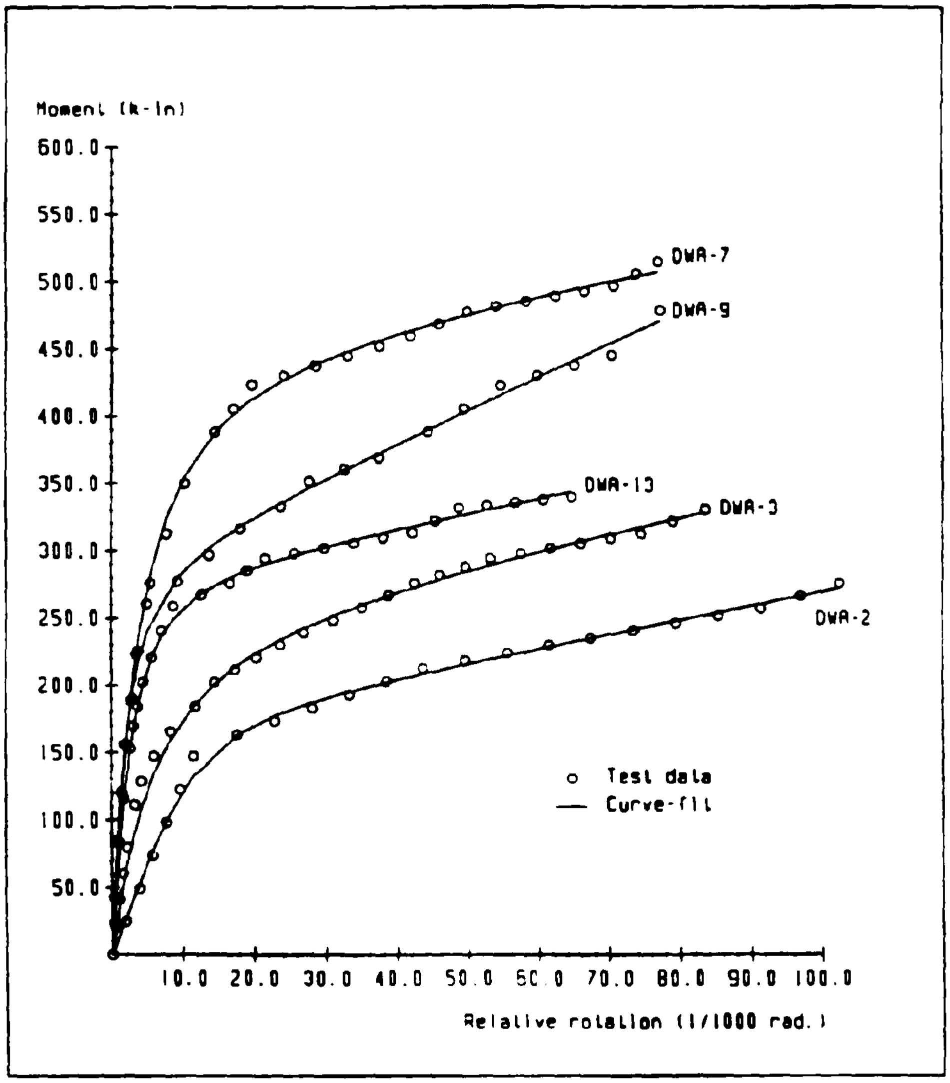

FIGURE A-2 Comparison Between Curve-fitting and Experimental Results for DWA Connections

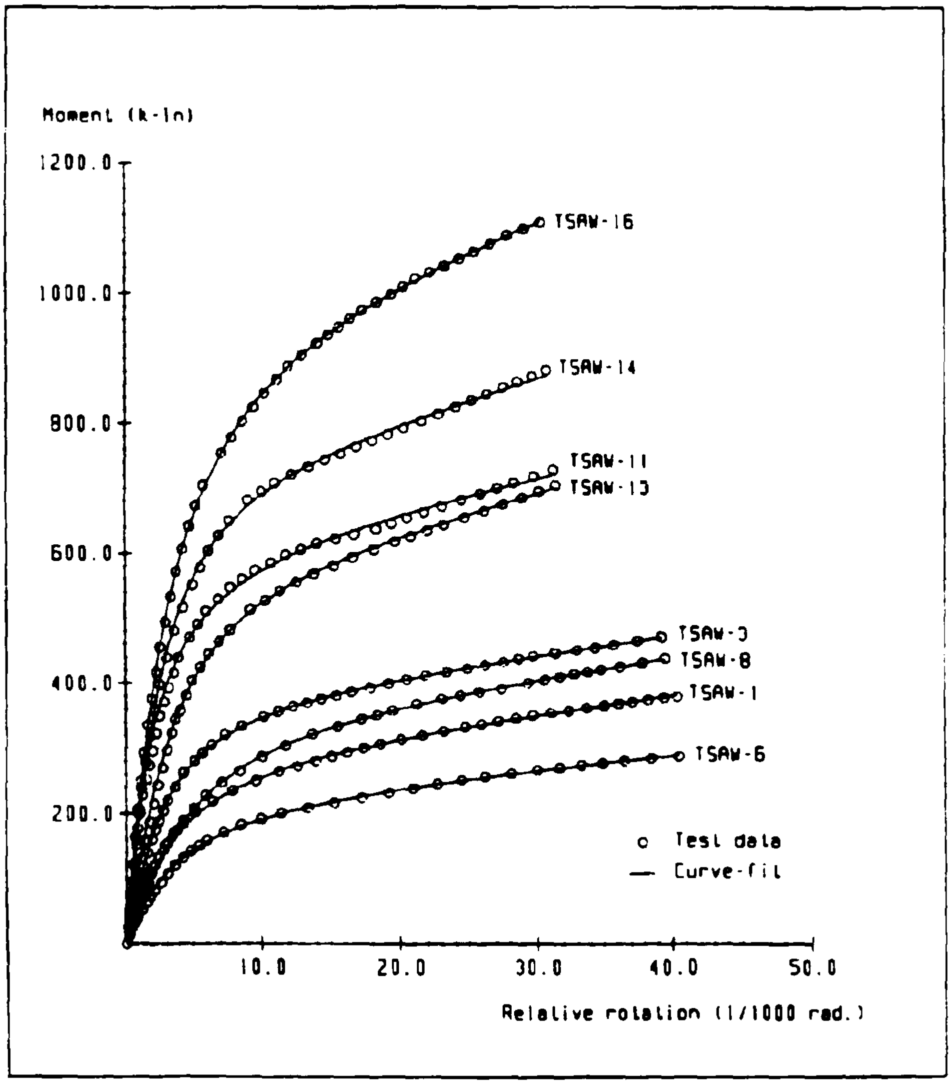

FIGURE A-3 Comparison Between Curve-fitting and Experimental Results for TSAW Connections

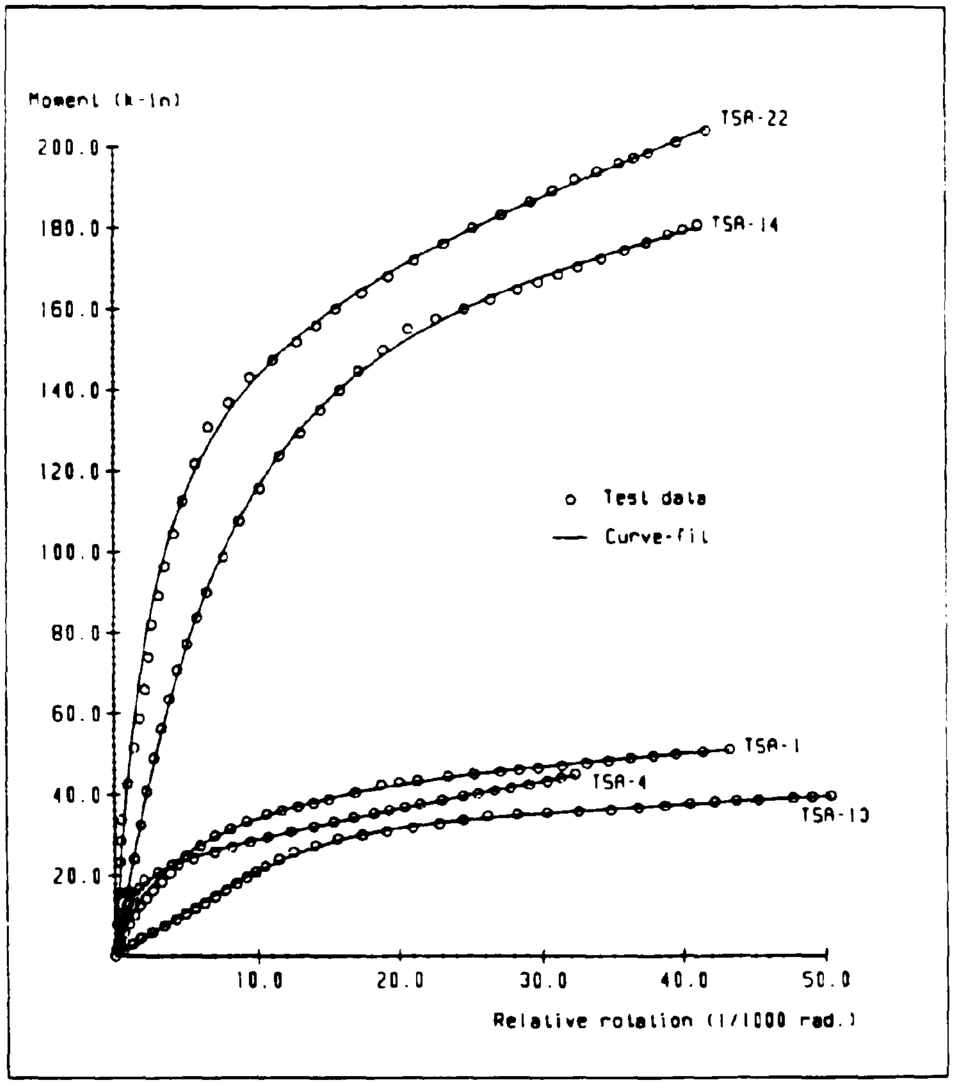

FIGURE A-4 Comparison Between Curve-fitting and Experimental for TSA Connections

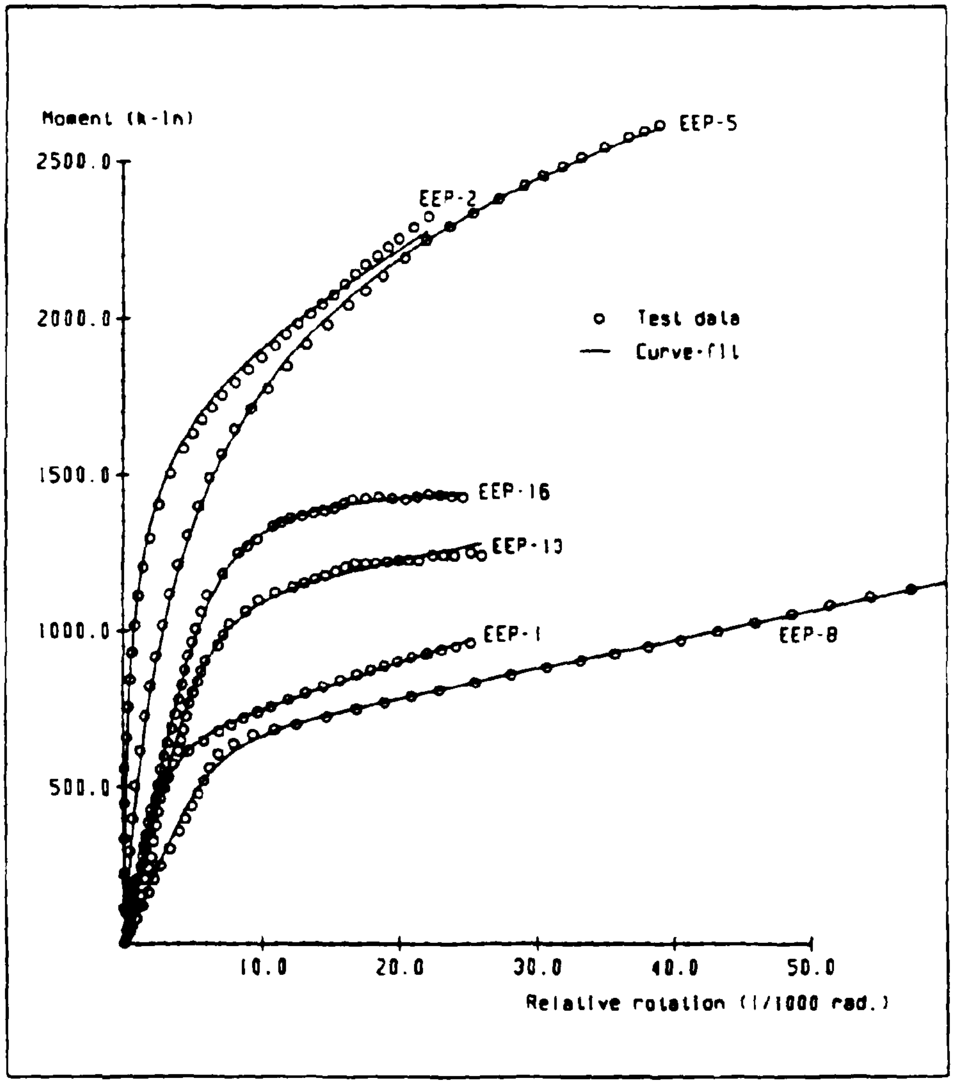

FIGURE A-5 Comparison Between Curve-fitting and Experimental Results for EEP Connections

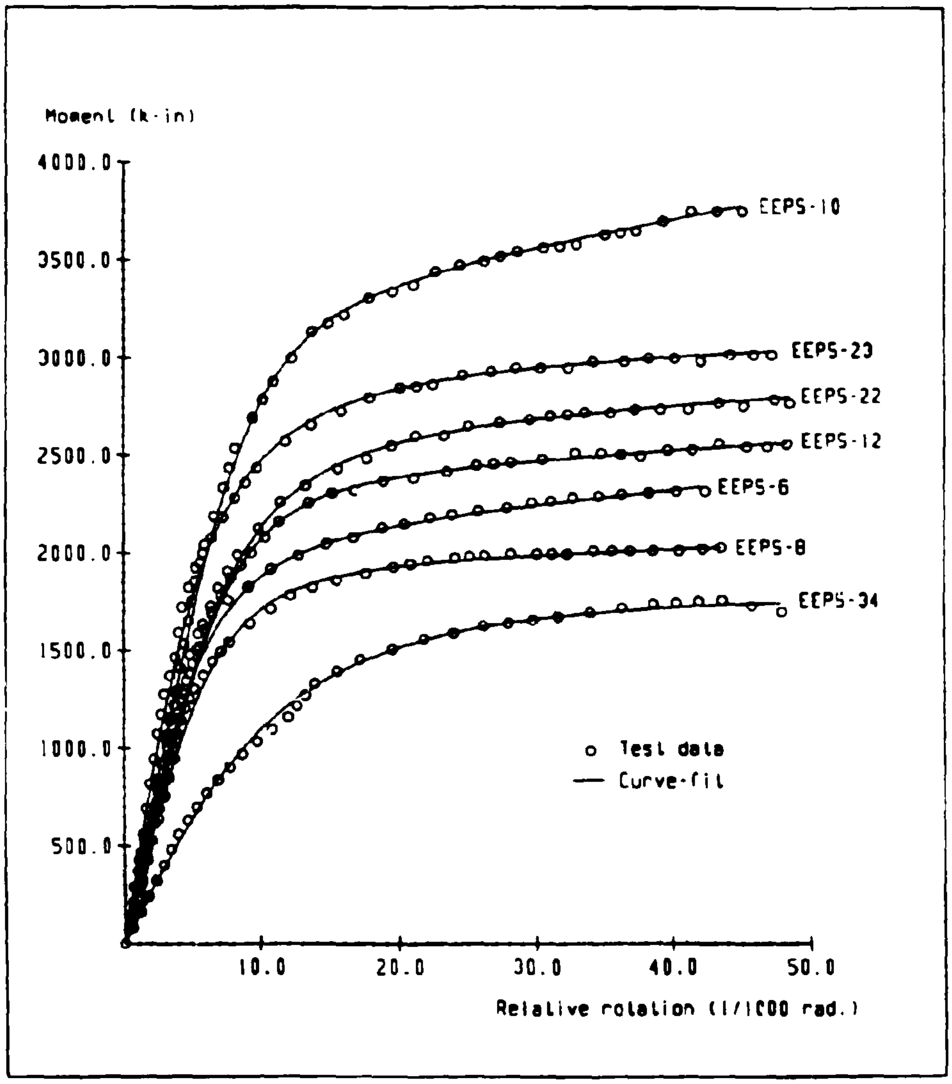

FIGURE A-6 Comparison Between Curve-fitting and Experimental Results for EEPS Connections

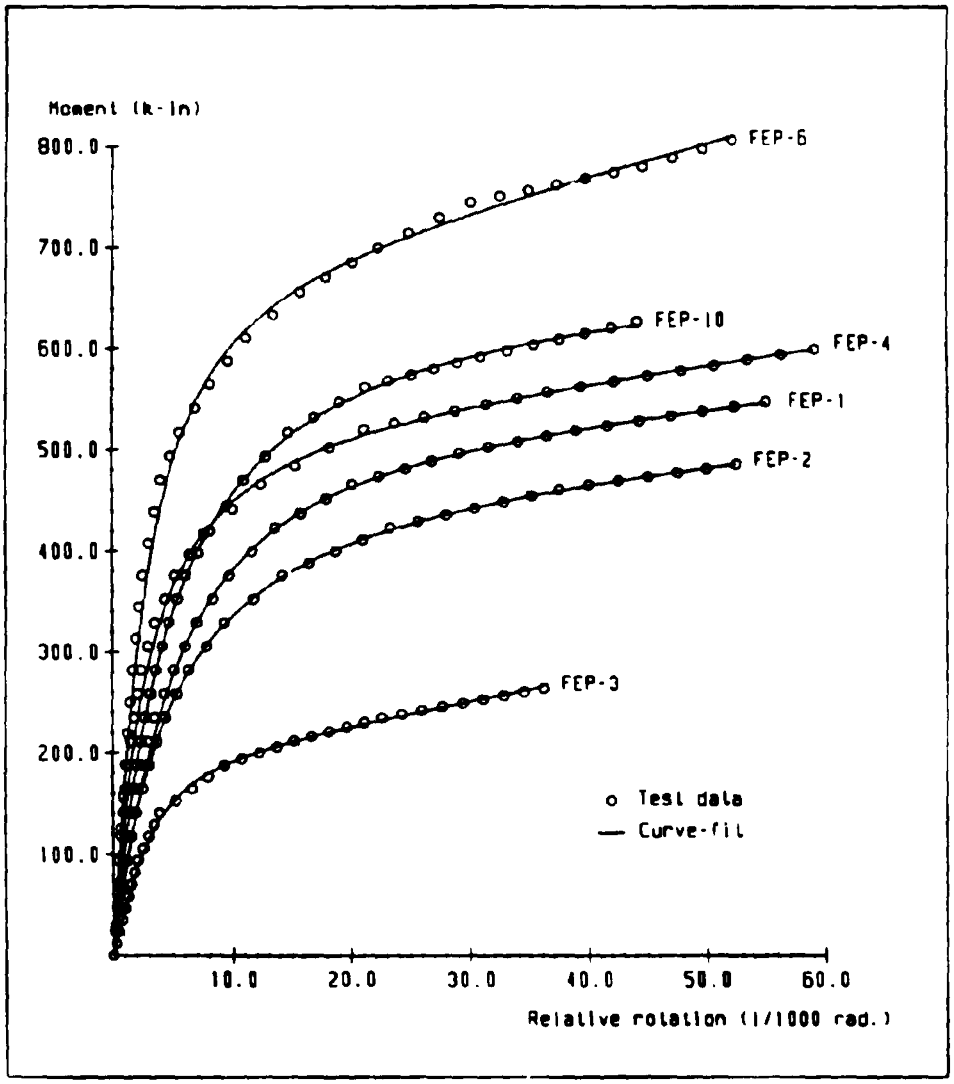

FIGURE A-7 Comparison Between Curve-fitting and Experimental Res..lts for FEP Connections

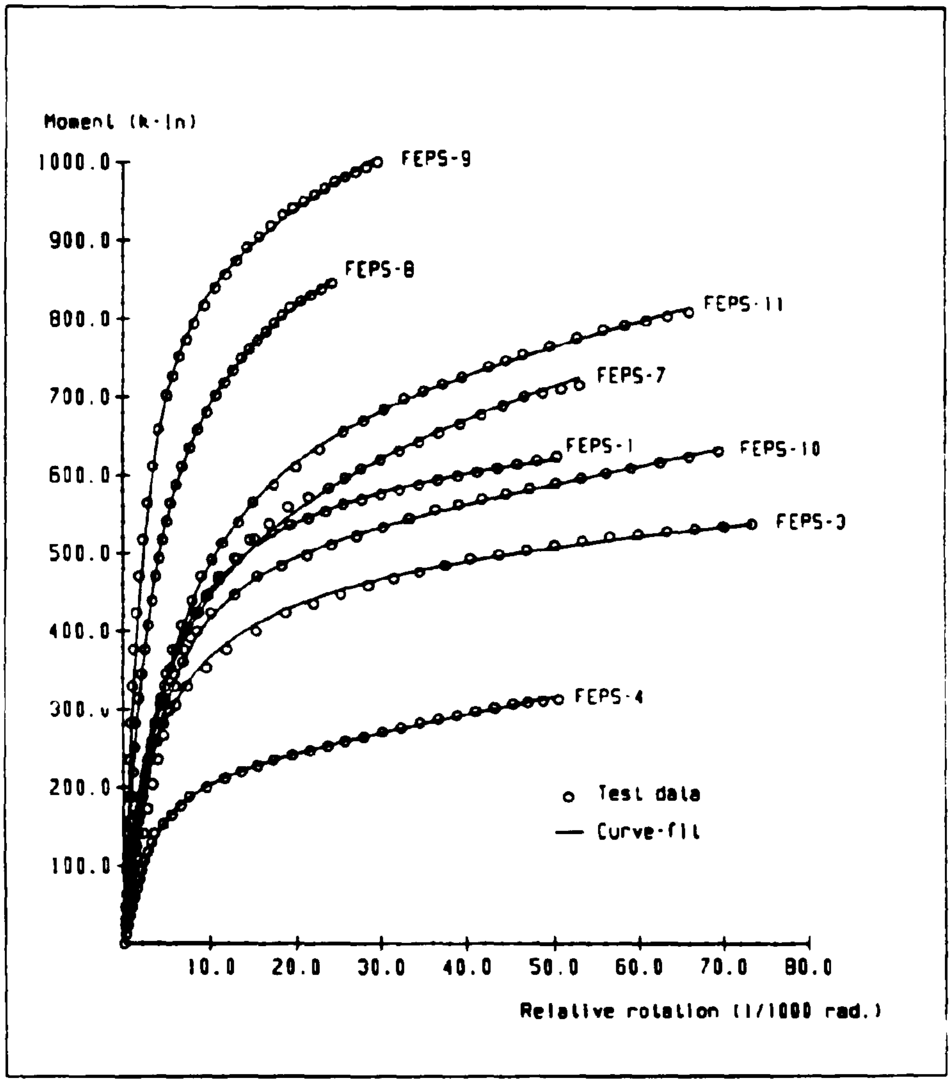

FIGURE A-8 Comparison Between Curve-fitting and Experimental Results for FEPS Connections

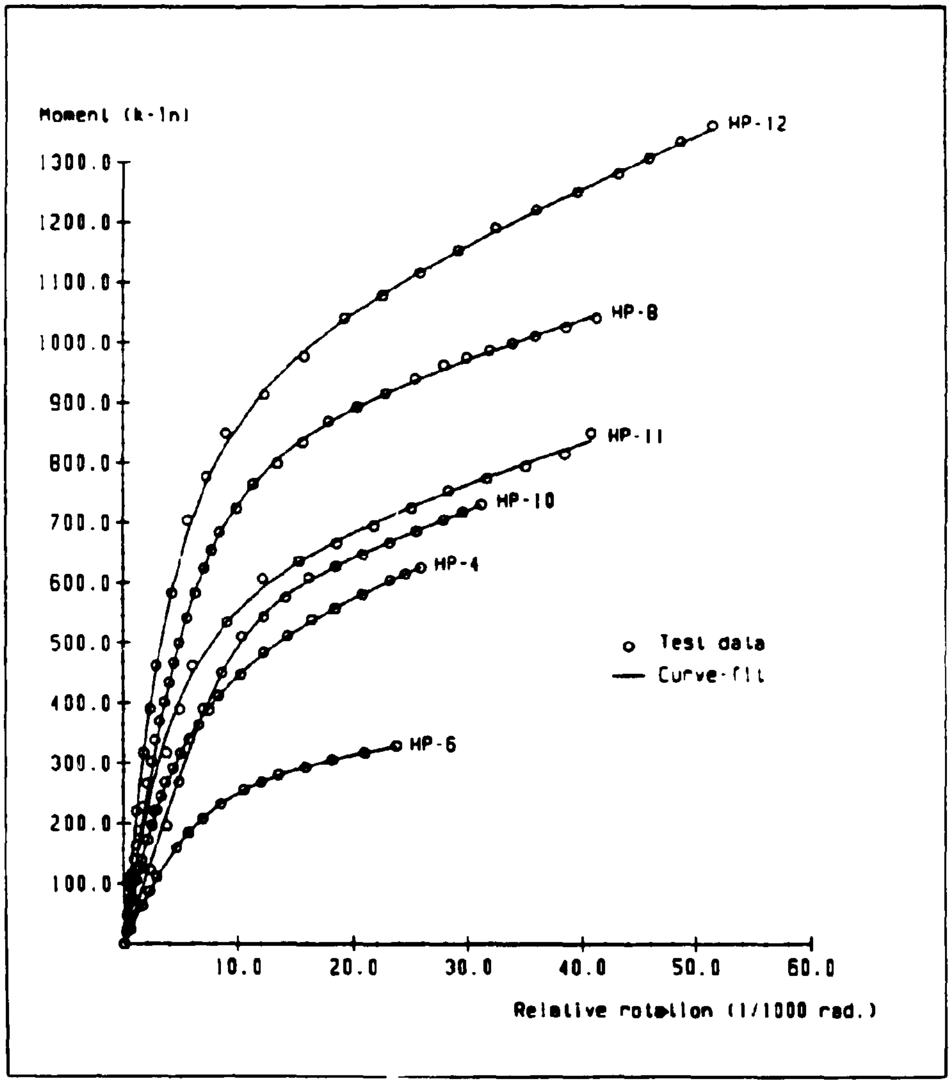

FIGURE A-9 Comparison Between Curve-fitting and Experimental Results for HP Connections

NATIONAL CENTER FOR EARTHQUAKE ENGINEERING RESEARCH
LIST OF TECHNICAL REPORTS

The National Center for Earthquake Engineering Research (NCEER) publishes technical reports on a variety of subjects related to earthquake engineering written by authors funded through NCEER. These reports are available from both NCEER's Publications Department and the National Technical Information Service (NTIS). Requests for reports should be directed to the Publications Department, National Center for Earthquake Engineering Research, State University of New York at Buffalo, Red Jacket Quadrangle, Buffalo, New York 14261. Reports can also be requested through NTIS, 5285 Port Royal Road, Springfield, Virginia 22161. NTIS accession numbers are shown in parenthesis, if available.

NCEER-87-0001 "First-Year Program in Research, Education and Technology Transfer," 3/5/87, (PB88-134275/AS).

NCEER-87-0002 "Experimental Evaluation of Instantaneous Optimal Algorithms for Structural Control," by R.C. Lin, T.T. Soong and A.M. Reinhorn, 4/20/87, (PB88-134341/AS).

NCEER-87-0003 "Experimentation Using the Earthquake Simulation Facilities at University at Buffalo," by A.M. Reinhorn and R.L. Ketter, to be published.

NCEER-87-0004 "The System Characteristics and Performance of a Shaking Table," by J.S. Hwang, K.C. Chang and G.C. Lee, 6/1/87, (PB88-134259/AS). This report is available only through NTIS (see address given above).

NCEER-87-0005 "A Finite Element Formulation for Nonlinear Viscoplastic Material Using a Q Model," by O. Gyebi and G. Dasgupta, 11/2/87, (PB88-213764/AS).

NCEER-87-0006 "Symbolic Manipulation Program (SMP) - Algebraic Codes for Two and Three Dimensional Finite Element Formulations," by X. Lee and G. Dasgupta, 11/9/87, (PB88-21?522/AS).

NCEER-87-0007 "Instantaneous Optimal Control Laws for Tall Buildings Under Seismic Excitations," by J.N. Yang, A. Akbarpour and P. Ghaemmaghami, 6/10/87, (PB88-134333/AS).

NCEER-87-0008 "IDARC: Inelastic Damage Analysis of Reinforced Concrete Frame - Shear-Wall Structures," by Y.J. Park, A.M. Reinhorn and S.K. Kunnath, 7/20/87, (PB88-134325/AS).

NCEER-87-0009 "Liquefaction Potential for New York State: A Preliminary Report on Sites in Manhattan and Buffalo," by M. Budhu, V. Vijayakumar, R.F. Giese and L. Baumgras, 8/31/87, (PB88-163704/AS). This report is available only through NTIS (see address given above).

NCEER-87-0010 "Vertical and Torsional Vibration of Foundations in Inhomogeneous Media," by A.S. Veletsos and K.W. Dotson, 6/1/87, (PB88-134291/AS).

NCEER-87-0011 "Seismic Probabilistic Risk Assessment and Seismic Margins Studies for Nuclear Power Plants," by Howard H.M. Hwang, 6/15/87, (PB88-134267/AS).

NCEER-87-0012 "Parametric Studies of Frequency Response of Secondary Systems Under Ground-Acceleration Excitations," by Y. Yong and Y.K. Lin, 6/10/87, (PB88-134309/AS).

NCEER-87-0013 "Frequency Response of Secondary Systems Under Seismic Excitation," by J.A. HoLung, J. Cai and Y.K. Lin, 7/31/87, (PB88-134317/AS).

NCEER-87-0014 "Modelling Earthquake Ground Motions in Seismically Active Regions Using Parametric Time Series Methods," by G.W. Ellis and A.S. Cakmak, 8/25/87, (PB88-134283/AS).

NCEER-87-0015 "Detection and Assessment of Seismic Structural Damage," by E. DiPasquale and A.S. Cakmak, 8/25/87, (PB88-163712/AS).

NCEER-87-0016 "Pipeline Experiment at Parkfield, California," by J. Isenberg and E. Richardson, 9/15/87, (PB88-163720/AS). This report is available only through NTIS (see address given above).

NCEER-87-0017	"Digital Simulation of Seismic Ground Motion," by M. Shinozuka, G. Deodatis and T. Harada, 8/31/87, (PB88-155197/AS). This report is available only through NTIS (see address given above).
NCEER-87-0018	"Practical Considerations for Structural Control: System Uncertainty, System Time Delay and Truncation of Small Control Forces," J.N. Yang and A. Akbarpour, 8/10/87, (PB88-163738/AS).
NCEER-87-0019	"Modal Analysis of Nonclassically Damped Structural Systems Using Canonical Transformation," by J.N. Yang, S. Sarkani and F.X. Long, 9/27/87, (PB88-187851/AS).
NCEER-87-0020	"A Nonstationary Solution in Random Vibration Theory," by J.R. Red-Horse and P.D. Spanos, 11/3/87, (PB88-163746/AS).
NCEER-87-0021	"Horizontal Impedances for Radially Inhomogeneous Viscoelastic Soil Layers," by A.S. Veletsos and K.W. Dotson, 10/15/87, (PB88-150859/AS).
NCEER-87-0022	"Seismic Damage Assessment of Reinforced Concrete Members," by Y.S. Chung, C. Meyer and M. Shinozuka, 10/9/87, (PB88-150867/AS). This report is available only through NTIS (see address given above).
NCEER-87-0023	"Active Structural Control in Civil Engineering," by T.T. Soong, 11/11/87, (PB88-187778/AS).
NCEER-87-0024	Vertical and Torsional Impedances for Radially Inhomogeneous Viscoelastic Soil Layers," by K.W. Dotson and A.S. Veletsos, 12/87, (PB88-187786/AS).
NCEER-87-0025	"Proceedings from the Symposium on Seismic Hazards, Ground Motions, Soil-Liquefaction and Engineering Practice in Eastern North America," October 20-22, 1987, edited by K.H. Jacob, 12/87, (PB88-188115/AS).
NCEER-87-0026	"Report on the Whittier-Narrows, California, Earthquake of October 1, 1987," by J. Pantelic and A. Reinhorn, 11/87, (PB88-187752/AS). This report is available only through NTIS (see address given above).
NCEER-87-0027	"Design of a Modular Program for Transient Nonlinear Analysis of Large 3-D Building Structures," by S. Srivastav and J.F. Abel, 12/30/87, (PB88-187950/AS).
NCEER-87-0028	"Second-Year Program in Research, Education and Technology Transfer," 3/8/88, (PB88-219480/AS).
NCEER-88-0001	"Workshop on Seismic Computer Analysis and Design of Buildings With Interactive Graphics," by W. McGuire, J.F. Abel and C.H. Conley, 1/18/88, (PB88-187760/AS).
NCEER-88-0002	"Optimal Control of Nonlinear Flexible Structures," by J.N. Yang, F.X. Long and D. Wong, 1/22/88, (PB88-213772/AS).
NCEER-88-0003	"Substructuring Techniques in the Time Domain for Primary-Secondary Structural Systems," by G.D. Manolis and G. Juhn, 2/10/88, (PB88-213780/AS).
NCEER-88-0004	"Iterative Seismic Analysis of Primary-Secondary Systems," by A. Singhal, L.D. Lutes and P.D. Spanos, 2/23/88, (PB88-213798/AS).
NCEER-88-0005	"Stochastic Finite Element Expansion for Random Media," by P.D. Spanos and R. Ghanem, 3/14/88, (PB88-213806/AS).
NCEER-88-0006	"Combining Structural Optimization and Structural Control," by F.Y. Cheng and C.P. Pantelides, 1/10/88, (PB88-213814/AS).
NCEER-88-0007	"Seismic Performance Assessment of Code-Designed Structures," by H.H-M. Hwang, J-W. Jaw and H-J. Shau, 3/20/88, (PB88-219423/AS).

NCEER-88-0008 "Reliability Analysis of Code-Designed Structures Under Natural Hazards," by H.H-M. Hwang, H. Ushiba and M. Shinozuka, 2/29/88, (PB88-229471/AS).

NCEER-88-0009 "Seismic Fragility Analysis of Shear Wall Structures," by J-W Jaw and H-H-M. Hwang, 4/30/88, (PB89-102867/AS).

NCEER-88-0010 "Base Isolation of a Multi-Story Building Under a Harmonic Ground Motion - A Comparison of Performances of Various Systems," by F-G Fan, G. Ahmadi and I.G. Tadjbakhsh, 5/18/88, (PB89-122238/AS).

NCEER-88-0011 "Seismic Floor Response Spectra for a Combined System by Green's Functions," by F.M. Lavelle, L.A. Bergman and P.D. Spanos, 5/1/88, (PB89-102875/AS).

NCEER-88-0012 "A New Solution Technique for Randomly Excited Hysteretic Structures," by G.Q. Cai and Y.K. Lin, 5/16/88, (PB89-102883/AS).

NCEER-88-0013 "A Study of Radiation Damping and Soil-Structure Interaction Effects in the Centrifuge," by K. Weissman, supervised by J.H. Prevost, 5/24/88, (PB89-144703/AS).

NCEER-88-0014 "Parameter Identification and Implementation of a Kinematic Plasticity Model for Frictional Soils," by J.H. Prevost and D.V. Griffiths, to be published.

NCEER-88-0015 "Two- and Three- Dimensional Dynamic Finite Element Analyses of the Long Valley Dam," by D.V. Griffiths and J.H. Prevost, 6/17/88, (PB89-144711/AS).

NCEER-88-0016 "Damage Assessment of Reinforced Concrete Structures in Eastern United States," by A.M. Reinhorn, M.J. Seidel, S.K. Kunnath and Y.J. Park, 6/15/88, (PB89-122220/AS).

NCEER-88-0017 "Dynamic Compliance of Vertically Loaded Strip Foundations in Multilayered Viscoelastic Soils," by S. Ahmad and A.S.M. Israil, 6/17/88, (PB89-102891/AS).

NCEER-88-0018 "An Experimental Study of Seismic Structural Response With Added Viscoelastic Dampers," by R.C. Lin, Z. Liang, T.T. Soong and R.H. Zhang, 6/30/88, (PB89-122212/AS).

NCEER-88-0019 "Experimental Investigation of Primary - Secondary System Interaction," by G.D. Manolis, G. Juhn and A.M. Reinhorn, 5/27/88, (PB89-122204/AS).

NCEER-88-0020 "A Response Spectrum Approach For Analysis of Nonclassically Damped Structures," by J.N. Yang, S. Sarkani and F.X. Long, 4/22/88, (PB89-102909/AS).

NCEER-88-0021 "Seismic Interaction of Structures and Soils: Stochastic Approach," by A.S. Veletsos and A.M. Prasad, 7/21/88, (PB89-122196/AS).

NCEER-88-0022 "Identification of the Serviceability Limit State and Detection of Seismic Structural Damage," by E. DiPasquale and A.S. Cakmak, 6/15/88, (PB89-122188/AS).

NCEER-88-0023 "Multi-Hazard Risk Analysis: Case of a Simple Offshore Structure," by B.K. Bhartia and E.H. Vanmarcke, 7/21/88, (PB89-145213/AS).

NCEER-88-0024 "Automated Seismic Design of Reinforced Concrete Buildings," by Y.S. Chung, C. Meyer and M. Shinozuka, 7/5/88, (PB89-122170/AS).

NCEER-88-0025 "Experimental Study of Active Control of MDOF Structures Under Seismic Excitations," by L.L. Chung, R.C. Lin, T.T. Soong and A.M. Reinhorn, 7/10/88, (PB89-122600/AS).

NCEER-88-0026 "Earthquake Simulation Tests of a Low-Rise Metal Structure," by J.S. Hwang, K.C. Chang, G.C. Lee and R.L. Ketter, 8/1/88, (PB89-102917/AS).

NCEER-88-0027 "Systems Study of Urban Response and Reconstruction Due to Catastrophic Earthquakes," by F. Kozin and H.K. Zhou, 9/22/88, (PB90-162348/AS).

NCEER-88-0028 "Seismic Fragility Analysis of Plane Frame Structures," by H.H-M. Hwang and Y.K. Low, 7/31/88, (PB89-131445/AS).

NCEER-88-0029 "Response Analysis of Stochastic Structures," by A. Kardara, C. Bucher and M. Shinozuka, 9/22/88, (PB89-174429/AS).

NCEER-88-0030 "Nonnormal Accelerations Due to Yielding in a Primary Structure," by D.C.K. Chen and L.D. Lutes, 9/19/88, (PB89-131437/AS).

NCEER-88-0031 "Design Approaches for Soil-Structure Interaction," by A.S. Veletsos, A.M. Prasad and Y. Tang, 12/30/88, (PB89-174437/AS).

NCEER-88-0032 "A Re-evaluation of Design Spectra for Seismic Damage Control," by C.J. Turkstra and A.G. Tallin, 11/7/88, (PB89-145221/AS).

NCEER-88-0033 "The Behavior and Design of Noncontact Lap Splices Subjected to Repeated Inelastic Tensile Loading," by V.E. Sagan, P. Gergely and R.N. White, 12/8/88, (PB89-163737/AS).

NCEER-88-0034 "Seismic Response of Pile Foundations," by S.M. Mamoon, P.K. Banerjee and S. Ahmad, 11/1/88, (PB89-145239/AS).

NCEER-88-0035 "Modeling of R/C Building Structures With Flexible Floor Diaphragms (IDARC2)," by A.M. Reinhorn, S.K. Kunnath and N. Panahshahi, 9/7/88, (PB89-207153/AS).

NCEER-88-0036 "Solution of the Dam-Reservoir Interaction Problem Using a Combination of FEM, BEM with Particular Integrals, Modal Analysis, and Substructuring," by C-S. Tsai, G.C. Lee and R.L. Ketter, 12/31/88, (PB89-207146/AS).

NCEER-88-0037 "Optimal Placement of Actuators for Structural Control," by F.Y. Cheng and C.P. Pantelides, 8/15/88, (PB89-162846/AS).

NCEER-88-0038 "Teflon Bearings in Aseismic Base Isolation: Experimental Studies and Mathematical Modeling," by A. Mokha, M.C. Constantinou and A.M. Reinhorn, 12/5/88, (PB89-218457/AS).

NCEER-88-0039 "Seismic Behavior of Flat Slab High-Rise Buildings in the New York City Area," by P. Weidlinger and M. Ettouney, 10/15/88, (PB90-145681/AS).

NCEER-88-0040 "Evaluation of the Earthquake Resistance of Existing Buildings in New York City," by P. Weidlinger and M. Ettouney, 10/15/88, to be published.

NCEER-88-0041 "Small-Scale Modeling Techniques for Reinforced Concrete Structures Subjected to Seismic Loads," by W. Kim, A. El-Attar and R.N. White, 11/22/88, (PB89-189625/AS).

NCEER-88-0042 "Modeling Strong Ground Motion from Multiple Event Earthquakes," by G.W. Ellis and A.S. Cakmak, 10/15/88, (PB89-174445/AS).

NCEER-88-0043 "Nonstationary Models of Seismic Ground Acceleration," by M. Grigoriu, S.E. Ruiz and E. Rosenblueth, 7/15/88, (PB89-189617/AS).

NCEER-88-0044 "SARCF User's Guide: Seismic Analysis of Reinforced Concrete Frames," by Y.S. Chung, C. Meyer and M. Shinozuka, 11/9/88, (PB89-174452/AS).

NCEER-88-0045 "First Expert Panel Meeting on Disaster Research and Planning," edited by J. Pantelic and J. Stoyle, 9/15/88, (PB89-174460/AS).

NCEER-88-0046 "Preliminary Studies of the Effect of Degrading Infill Walls on the Nonlinear Seismic Response of Steel Frames," by C.Z. Chrysostomou, P. Gergely and J.F. Abel, 12/19/88, (PB89-208383/AS).

NCEER-88-0047 "Reinforced Concrete Frame Component Testing Facility - Design, Construction, Instrumentation and Operation," by S.P. Pessiki, C. Conley, T. Bond, P. Gergely and R.N. White, 12/16/88, (PB89-174478/AS).

NCEER-89-0001 "Effects of Protective Cushion and Soil Compliancy on the Response of Equipment Within a Seismically Excited Building," by J.A. HoLung, 2/16/89, (PB89-207179/AS).

NCEER-89-0002 "Statistical Evaluation of Response Modification Factors for Reinforced Concrete Structures," by H.H-M. Hwang and J-W. Jaw, 2/17/89, (PB89-207187/AS).

NCEER-89-0003 "Hysteretic Columns Under Random Excitation," by G-Q. Cai and Y.K. Lin, 1/9/89, (PB89-196513/AS).

NCEER-89-0004 "Experimental Study of 'Elephant Foot Bulge' Instability of Thin-Walled Metal Tanks," by Z-H. Jia and R.L. Ketter, 2/22/89, (PB89-207195/AS).

NCEER-89-0005 "Experiment on Performance of Buried Pipelines Across San Andreas Fault," by J. Isenberg, E. Richardson and T.D. O'Rourke, 3/10/89, (PB89-218440/AS).

NCEER-89-0006 "A Knowledge-Based Approach to Structural Design of Earthquake-Resistant Buildings," by M. Subramani, P. Gergely, C.H. Conley, J.F. Abel and A.H. Zaghw, 1/15/89, (PB89-218465/AS).

NCEER-89-0007 "Liquefaction Hazards and Their Effects on Buried Pipelines," by T.D. O'Rourke and P.A. Lane, 2/1/89, (PB89-218481).

NCEER-89-0008 "Fundamentals of System Identification in Structural Dynamics," by H. Imai, C-B. Yun, O. Maruyama and M. Shinozuka, 1/26/89, (PB89-207211/AS).

NCEER-89-0009 "Effects of the 1985 Michoacan Earthquake on Water Systems and Other Buried Lifelines in Mexico," by A.G. Ayala and M.J. O'Rourke, 3/8/89, (PB89-207229/AS).

NCEER-89-R010 "NCEER Bibliography of Earthquake Education Materials," by K.E.K. Ross, Second Revision, 9/1/89, (PB90-125352/AS).

NCEER-89-0011 "Inelastic Three-Dimensional Response Analysis of Reinforced Concrete Building Structures (IDARC-3D), Part I - Modeling," by S.K. Kunnath and A.M. Reinhorn, 4/17/89, (PB90-114612/AS).

NCEEP-89-0012 "Recommended Modifications to ATC-14," by C.D. Poland and J.O. Malley, 4/12/89, (PB90-108648/AS).

NCEER-89-0013 "Repair and Strengthening of Beam-to-Column Connections Subjected to Earthquake Loading," by M. Corazao and A.J. Durrani, 2/28/89, (PB90-109885/AS).

NCEER-89-0014 "Program EXKAL2 for Identification of Structural Dynamic Systems," by O. Maruyama, C-B. Yun, M. Hoshiya and M. Shinozuka, 5/19/89, (PB90-109877/AS).

NCEER-89-0015 "Response of Frames With Bolted Semi-Rigid Connections, Part I - Experimental Study and Analytical Predictions," by P.J. DiCorso, A.M. Reinhorn, J.R. Dickerson, J.B. Radziminski and W.L. Harper, 6/1/89, to be published.

NCEER-89-0016 "ARMA Monte Carlo Simulation in Probabilistic Structural Analysis," by P.D. Spanos and M.P. Mignolet, 7/10/89, (PB90-109893/AS).

NCEER-89-P017 "Preliminary Proceedings from the Conference on Disaster Preparedness - The Place of Earthquake Education in Our Schools," Edited by K.E.K. Ross, 6/23/89.

NCEER-89-0017 "Proceedings from the Conference on Disaster Preparedness - The Place of Earthquake Education in Our Schools," Edited by K.E.K. Ross, 12/31/89, (PB90-207895).

NCEER-89-0018 "Multidimensional Models of Hysteretic Material Behavior for Vibration Analysis of Shape Memory Energy Absorbing Devices, by E.J. Graesser and F.A. Cozzarelli, 6/7/89, (PB90-164146/AS).

NCEER-89-0019 "Nonlinear Dynamic Analysis of Three-Dimensional Base Isolated Structures (3D-BASIS)," by S. Nagarajaiah, A.M. Reinhorn and M.C. Constantinou, 8/3/89, (PB90-161936/AS).

NCEER-89-0020 "Structural Control Considering Time-Rate of Control Forces and Control Rate Constraints," by F.Y. Cheng and C.P. Pantelides, 8/3/89, (PB90-120445/AS).

NCEER-89-0021 "Subsurface Conditions of Memphis and Shelby County," by K.W. Ng, T-S. Chang and H-H.M. Hwang, 7/26/89, (PB90-120437/AS).

NCEER-89-0022 "Seismic Wave Propagation Effects on Straight Jointed Buried Pipelines," by K. Elhmadi and M.J. O'Rourke, 8/24/89, (PB90-162322/AS).

NCEER-89-0023 "Workshop on Serviceability Analysis of Water Delivery Systems," edited by M. Grigoriu, 3/6/89, (PB90-127424/AS).

NCEER-89-0024 "Shaking Table Study of a 1/5 Scale Steel Frame Composed of Tapered Members," by K.C. Chang, J.S. Hwang and G.C. Lee, 9/18/89, (PB90-160169/AS).

NCEER-89-0025 "DYNA1D: A Computer Program for Nonlinear Seismic Site Response Analysis - Technical Documentation," by Jean H. Prevost, 9/14/89, (PB90-161944/AS).

NCEER-89-0026 "1:4 Scale Model Studies of Active Tendon Systems and Active Mass Dampers for Aseismic Protection," by A.M. Reinhorn, T.T. Soong, R.C. Lin, Y.P. Yang, Y. Fukao, H. Abe and M. Nakai, 9/15/89, (PB90-173246/AS).

NCEER-89-0027 "Scattering of Waves by Inclusions in a Nonhomogeneous Elastic Half Space Solved by Boundary Element Methods," by P.K. Hadley, A. Askar and A.S. Cakmak, 6/15/89, (PB90-145699/AS).

NCEER-89-0028 "Statistical Evaluation of Deflection Amplification Factors for Reinforced Concrete Structures," by H.H.M. Hwang, J-W. Jaw and A.L. Ch'ng, 8/31/89, (PB90-164633/AS).

NCEER-89-0029 "Bedrock Accelerations in Memphis Area Due to Large New Madrid Earthquakes," by H.H.M. Hwang, C.H.S. Chen and G. Yu, 11/7/89, (PB90-162330/AS).

NCEER-89-0030 "Seismic Behavior and Response Sensitivity of Secondary Structural Systems," by Y.Q. Chen and T.T. Soong, 10/23/89, (PB90-164658/AS).

NCEER-89-0031 "Random Vibration and Reliability Analysis of Primary-Secondary Structural Systems," by Y. Ibrahim, M. Grigoriu and T.T. Soong, 11/10/89, (PB90-161951/AS).

NCEER-89-0032 "Proceedings from the Second U.S. - Japan Workshop on Liquefaction, Large Ground Deformation and Their Effects on Lifelines, September 26-29, 1989," Edited by T.D. O'Rourke and M. Hamada, 12/1/89, (PB90-209388/AS).

NCEER-89-0033 "Deterministic Model for Seismic Damage Evaluation of Reinforced Concrete Structures," by J.M. Bracci, A.M. Reinhorn, J.B. Mander and S.K. Kunnath, 9/27/89.

NCEER-89-0034 "On the Relation Between Local and Global Damage Indices," by E. DiPasquale and A.S. Cakmak, 8/15/89, (PB90-173865).

NCEER-89-0035 "Cyclic Undrained Behavior of Nonplastic and Low Plasticity Silts," by A.J. Walker and H.E. Stewart, 7/26/89, (PB90-183518/AS).

NCEER-89-0036 "Liquefaction Potential of Surficial Deposits in the City of Buffalo, New York," by M. Budhu, R. Giese and L. Baumgrass, 1/17/89, (PB90-208455/AS).

NCEER-89-0037 "A Deterministic Assessment of Effects of Ground Motion Incoherence," by A.S. Veletsos and Y. Tang, 7/15/89, (PB90-164294/AS).

NCEER-89-0038 "Workshop on Ground Motion Parameters for Seismic Hazard Mapping," July 17-18, 1989, edited by R.V. Whitman, 12/1/89, (PB90-173923/AS).

NCEER-89-0039 "Seismic Effects on Elevated Transit Lines of the New York City Transit Authority," by C.J. Costantino, C.A. Miller and E. Heymsfield, 12/26/89, (PB90-207887/AS).

NCEER-89-0040 "Centrifugal Modeling of Dynamic Soil-Structure Interaction," by K. Weissman, Supervised by J.H. Prevost, 5/10/89, (PB90-207879/AS).

NCEER-89-0041 "Linearized Identification of Buildings With Cores for Seismic Vulnerability Assessment," by I-K. Ho and A.E. Aktan, 11/1/89, (PB90-251943/AS).

NCEER-90-0001 "Geotechnical and Lifeline Aspects of the October 17, 1989 Loma Prieta Earthquake in San Francisco," by T.D. O'Rourke, H.E. Stewart, F.T. Blackburn and T.S. Dickerman, 1/90, (PB90-208596/AS).

NCEER-90-0002 "Nonnormal Secondary Response Due to Yielding in a Primary Structure," by D.C.K. Chen and L.D. Lutes, 2/28/90, (PB90-251976/AS).

NCEER-90-0003 "Earthquake Education Materials for Grades K-12," by K.E.K. Ross, 4/16/90, (PB91-113415/AS).

NCEER-90-0004 "Catalog of Strong Motion Stations in Eastern North America," by R.W. Busby, 4/3/90, (PB90-251984)/AS.

NCEER-90-0005 "NCEER Strong-Motion Data Base: A User Manuel for the GeoBase Release (Version 1.0 for the Sun3)," by P. Friberg and K. Jacob, 3/31/90 (PB90-258062/AS).

NCEER-90-0006 "Seismic Hazard Along a Crude Oil Pipeline in the Event of an 1811-1812 Type New Madrid Earthquake," by H.H.M. Hwang and C-H.S. Chen, 4/16/90(PB90-258054).

NCEER-90-0007 "Site-Specific Response Spectra for Memphis Sheahan Pumping Station," by H.H.M. Hwang and C.S. Lee, 5/15/90, (PB91-108811/AS).

NCEER-90-0008 "Pilot Study on Seismic Vulnerability of Crude Oil Transmission Systems," by T. Ariman, R. Dobry, M. Grigoriu, F. Kozin, M. O'Rourke, T. O'Rourke and M. Shinozuka, 5/25/90, (PB91-108837/AS).

NCEER-90-0009 "A Program to Generate Site Dependent Time Histories: EQGEN," by G.W. Ellis, M. Srinivasan and A.S. Cakmak, 1/30/90, (PB91-1108829/AS).

NCEER-90-0010 "Active Isolation for Seismic Protection of Operating Rooms," by M.E. Talbott, Supervised by M. Shinozuka, 6/8/9, (PB91-110205/AS).

NCEER-90-0011 "Program LINEARID for Identification of Linear Structural Dynamic Systems," by C-B. Yun and M. Shinozuka, 6/25/90, (PB91-110312/AS).

NCEER-90-0012 "Two-Dimensional Two-Phase Elasto-Plastic Seismic Response of Earth Dams," by A.N. Yiagos, Supervised by J.H. Prevost, 6/20/90, (PB91-110197/AS).

NCEER-90-0013 "Secondary Systems in Base-Isolated Structures: Experimental Investigation, Stochastic Response and Stochastic Sensitivity," by G.D. Manolis, G. Juhn, M.C. Constantinou and A.M. Reinhorn, 7/1/90, (PB91-110320/AS).

NCEER-90-0014 "Seismic Behavior of Lightly-Reinforced Concrete Column and Beam-Column Joint Details," by S.P. Pessiki, C.H. Conley, P. Gergely and R.N. White, 8/22/90, (PB91-108795/AS).

NCEER-90-0015 "Two Hybrid Control Systems for Building Structures Under Strong Earthquakes," by J.N. Yang and A. Danielians, 6/29/90, (FB91-125393/AS).

NCEER-90-0016	"Instantaneous Optimal Control with Acceleration and Velocity Feedback," by J.N. Yang and Z. Li, 6/29/90, (PB91-125401/AS).
NCEER-90-0017	"Reconnaissance Report on the Northern Iran Earthquake of June 21, 1990," by M. Mehrain, 10/4/90, (PB91-125377/AS).
NCEER-90-0018	"Evaluation of Liquefaction Potential in Memphis and Shelby County," by T.S. Chang, P.S. Tang, C.S. Lee and H. Hwang, 8/10/90, (PB91-125427/AS).
NCEER-90-0019	"Experimental and Analytical Study of a Combined Sliding Disc Bearing and Helical Steel Spring Isolation System," by M.C. Constantinou, A.S. Mokha and A.M. Reinhorn, 10/4/90, (PB91-125385/AS).
NCEER-90-0020	"Experimental Study and Analytical Prediction of Earthquake Response of a Sliding Isolation System with a Spherical Surface," by A.S. Mokha, M.C. Constantinou and A.M. Reinhorn, 10/11/90, (PB91-125419/AS).
NCEER-90-0021	"Dynamic Interaction Factors for Floating Pile Groups," by G. Gazetas, K. Fan, A. Kaynia and E. Kausel, 9/10/90, (PB91-170381/AS).
NCEER-90-0022	"Evaluation of Seismic Damage Indices for Reinforced Concrete Structures," by S. Rodríguez-Gómez and A.S. Cakmak, 9/30/90, PB91-171322/AS).
NCEER-90-0023	"Study of Site Response at a Selected Memphis Site," by H. Desai, S. Ahmad, E.S. Gazetas and M.R. Oh, 10/11/90.
NCEER-90-0024	"A User's Guide to Strongmo: Version 1.0 of NCEER's Strong-Motion Data Access Tool for PCs and Terminals," by P.A. Friberg and C.A.T. Susch, 11/15/90, (PB91-171272/AS).
NCEER-90-0025	"A Three-Dimensional Analytical Study of Spatial Variability of Seismic Ground Motions," by L-L. Hong and A.H.-S. Ang, 10/30/90, (PB91-170399/AS).
NCEER-90-0026	"MUMOID User's Guide - A Program for the Identification of Modal Parameters," by S. Rodríguez-Gómez and E. DiPasquale, 9/30/90, (PB91-171298/AS).
NCEER-90-0027	"SARCF-II User's Guide - Seismic Analysis of Reinforced Concrete Frames," by S. Rodríguez-Gómez, Y.S. Chung and C. Meyer, 9/30/90.
NCEER-90-0028	"Viscous Dampers: Testing, Modeling and Application in Vibration and Seismic Isolation," by N. Makris and M.C. Constantinou, 12/20/90 (PB91-190561/AS).
NCEER-90-0029	"Soil Effects on Earthquake Ground Motions in the Memphis Area," by H. Hwang, C.S. Lee, K.W. Ng and T.S. Chang, 8/2/90, (PB91-190751/AS).
NCEER-91-0001	"Proceedings from the Third Japan-U.S. Workshop on Earthquake Resistant Design of Lifeline Facilities and Countermeasures for Soil Liquefaction, December 17-19, 1990," edited by T.D. O'Rourke and M. Hamada, 2/1/91, (PB91-179259/AS).
NCEER-91-0002	"Physical Space Solutions of Non-Proportionally Damped Systems," by M. Tong, Z. Liang and G.C. Lee, 1/15/91, (PB91-179242/AS).
NCEER-91-0003	"Kinematic Seismic Response of Single Piles and Pile Groups," by K. Fan, G. Gazetas, A. Kaynia, E. Kausel and S. Ahmad, 1/10/91, to be published.
NCEER-91-0004	"Theory of Complex Damping," by Z. Liang and G. Lee, to be published.
NCEER-91-0005	"3D-BASIS - Nonlinear Dynamic Analysis of Three Dimensional Base Isolated Structures: Part II," by S. Nagarajaiah, A.M. Reinhorn and M.C. Constantinou, 2/28/91, (PB91-190553/AS).

NCEER-91-0006 "A Multidimensional Hysteretic Model for Plasticity Deforming Metals in Energy Absorbing Devices," by E.J. Graesser and F.A. Cozzarelli, 4/9/91.

NCEER-91-0007 "A Framework for Customizable Knowledge-Based Expert Systems with an Application to a KBES for Evaluating the Seismic Resistance of Existing Buildings," by E.G. Ibarra Anaya and S.J. Fenves, 4/9/91.

NCEER-91-0008 "Nonlinear Analysis of Steel Frames with Semi-Rigid Connections Using the Capacity Spectrum Method," by G.G. Deierlein, S-H. Hsieh, Y-J. Shen and J.F. Abel, 7/2/91.